



Contents lists available at ScienceDirect



Tutorial

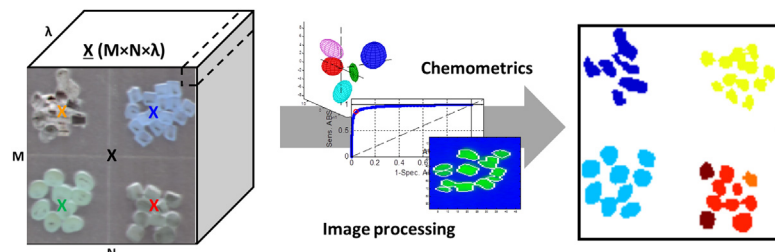
Hyperspectral image analysis. A tutorial

José Manuel Amigo ^{a,*}, Hamid Babamoradi ^a, Saioa Elcoroaristizabal ^{a,b}^a Spectroscopy and Chemometrics Group, Department of Food Sciences, Faculty of Science, University of Copenhagen, Rolighedsvej 30, Frederiksberg C DK-1958, Denmark^b Chemical and Environmental Engineering Department, School of Engineering, University of the Basque Country, Alameda de Urquijo s/n, E-48013 Bilbao, Spain

HIGHLIGHTS

- Comprehensive tutorial of Hyperspectral Image analysis.
- Hierarchical discrimination of six classes of plastics containing flame retardant.
- Step by step guidelines to perform class-modeling on hyperspectral images.
- Fusion of multivariate data analysis and digital image processing methods.
- Promising methodology for real-time detection of plastics containing flame retardant.

GRAPHICAL ABSTRACT



ARTICLE INFO

Article history:

Received 1 June 2015

Received in revised form

8 September 2015

Accepted 12 September 2015

Available online xxxx

Keywords:

Hyperspectral

Near infrared

Chemometrics

Classification

Plastic sorting

Flame retardant

ABSTRACT

This tutorial aims at providing guidelines and practical tools to assist with the analysis of hyperspectral images. Topics like hyperspectral image acquisition, image pre-processing, multivariate exploratory analysis, hyperspectral image resolution, classification and final digital image processing will be exposed, and some guidelines given and discussed.

Due to the broad character of current applications and the vast number of multivariate methods available, this paper has focused on an industrial chemical framework to explain, in a step-wise manner, how to develop a classification methodology to differentiate between several types of plastics by using Near infrared hyperspectral imaging and Partial Least Squares – Discriminant Analysis. Thus, the reader is guided through every single step and oriented in order to adapt those strategies to the user's case.

© 2015 Elsevier B.V. All rights reserved.

1. Hyperspectral imaging

Hyperspectral Imaging started in the early 70's with mainly applications on remote sensing [1–4]. It was much afterwards

when it started blooming in many other different disciplines like e.g. pharmaceutical research [5–11], pharmaceutical production [12–17], food sciences [18–22], food quality assurance [23–31], forensic sciences [32–37], biochemistry and biomedicine [38–40], or cultural heritage [41,42], among others. Clearly, the feasibility of a technique able to measure a whole spectrum (in different spectral modalities e.g. Near Infrared, Middle Infrared, Raman, Ultra-violet–Visible, Fluorescence, Terahertz [43] or even Magnetic

* Corresponding author.

E-mail address: jmar@food.ku.dk (J.M. Amigo).

Resonance [44,45]) for every single pixel in which the sample is divided, has been made it very attractive for many different applications. This breakthrough has been due to the close synergy between the tremendous evolution of faster, more reliable and more robust optical devices, and the implementation of powerful algorithms for processing hyperspectral images. The final aim of hyperspectral image analysis is to obtain a picture containing selective and specific information (quantitative, groups or spatial distribution) of the conforming compounds of the surface measured. Leaving apart the applications where this selective picture can be extracted by depicting the intensity of one single wavelength (sometimes found in Raman hyperspectral images), hyperspectral analysis is inherently linked to multivariate data analysis (a.k.a. chemometrics). Thus, the big success of hyperspectral imaging could not be understood without referring to the, sometimes overwhelming, implementation of different algorithms to handle all the data generated for a single image.

Chemometrics is a well-known discipline that allows extracting the information from data in a multivariate manner. Many reviews have been published pointing out the main multivariate or statistical methods to be applied in hyperspectral imaging for different purposes [5–9,18,46–52], as well as their main benefits and drawbacks; but sometimes it becomes cumbersome to know exactly which multivariate method is the most appropriate for every single type of purpose.

This tutorial is aimed at shedding light on the, sometimes, difficult task of performing a multivariate analysis on a hyperspectral image. Acknowledging that discussing all treatment options could be too long, here the major issues that a researcher faces while analyzing hyperspectral images are found and several feasible solutions are put forward. In order to follow a conducting thread, this tutorial will be focused on the development of a hierarchical multivariate classification model for plastic sorting containing flame retardants. This will help to set a chemical framework that covers two main points in hyperspectral imaging: 1) classification as one of the main application domains of hyperspectral imaging; and 2) the more and more common presence of hyperspectral cameras installed in industrial plants [53–56].

The manuscript has been divided into nine main sections, including the introductory Section 1. Section 2 is merely aimed at introducing the problematic of sorting plastics containing flame retardants. Section 3 describes the materials used and also offers several hints of the types of hyperspectral cameras and the software that the user can find available. The structure of a hyperspectral image from a chemical point of view is explained in Section 4. Section 5 describes in a comprehensive manner the main steps to follow when analyzing hyperspectral images. Special emphasis is given to discuss the main features of spectral and spatial pre-processing methods. Moreover, important topics like hyperspectral image exploration and resolution are discussed here. Since the main chemical framework is the development of a hierarchical classification model for different plastics containing flame retardant, Sections 6–8 are devoted to show the implementation of the classification models in a step-by-step manner. Here, the implementation of several digital image methods to discern between objects in an image is also explained (Section 8). The final Section 9 remarks different fundamental questions in hyperspectral imaging and gives some ideas of how to handle some acquisition and analysis issues.

2. Detection of flame retardants in plastics

Flame retardants (FRs) are organic compounds added to the plastics to increase the resistance to ignition, reduce flame spreading, suppress smoke formation, and prevent a polymer from

dripping [57]. Among all, Brominated FRs (BFRs) constitute a diverse group of FRs for minimizing fire hazards. BFRs are cost-effective and offer a high degree of processability, making them the most commonly used FRs in plastics. However, BFRs cause major environmental problems, thus, waste objects containing BFRs must be automatically identified and removed.

Identification of BFRs in plastics has been successfully accomplished using many methods such as Infrared Spectroscopy [58], Raman spectroscopy [59], Laser-Induced Breakdown Spectrometry (LIBS) [60], Sliding spark spectroscopy [61], X-Ray Fluorescence spectroscopy (XRF) [62], and chromatography [63]. Despite this progress, many of these methods are slow, expensive, and difficult to implement in a real-time framework, which make them unsuitable for automated sorting systems. In contrast, near infrared spectroscopy (NIR) is extensively used for automatic sorting due to fast scanning abilities, relative low cost and non-destructive nature. Nevertheless, successful identification of BFRs using NIR spectroscopy has not been reported yet.

Considering all this, this paper aims at showing how successful classification models can be created using Hyperspectral-NIR cameras to discriminate between different plastics containing variable amounts of BFRs. This will allow us to create different models using NIR for automatic sorting of plastics with critical additives at a rate of several parts per second, in order to implement an economically feasible recycling process that meets the major requirement of the industry.

3. Materials and methods

3.1. Materials

The plastics used in this study were kindly provided by the INNOSORT consortium (<http://innosort.teknologisk.dk/>). Five different plastics were supplied (Fig. 1a): acrylonitrile butadiene styrene (ABS), polyamide 6 (PA6), polybutylene terephthalate (PBT), polypropylene (PP) and polystyrene (PS). These plastics were produced in the shape of small pellets (of around 5 mm of diameter). The reference plastic for each category (i.e. without BFRs addition) was labeled as REF. All plastics were also doped in the manufacturing process with variable amounts of brominated flame retardants (BFRs) (Fig. 1b) between the boundaries of the corresponding legislation (due to confidentiality reasons and different research ongoing, the type and doped amount of BFR cannot be provided). In total, they comprised 14 different categories of plastics (5 main categories and 8 sub-categories) summarized in Table 1.

For the sake of clarity, Sections 4 and 5 will be illustrated using a small part of the hyperspectral image presented in Fig. 1a (red dashed square in the left part of Fig. 1a). This part is better illustrated in Fig. 2.

3.2. Measurements

There are many types of hyperspectral cameras in the market, depending on the type of radiation (UV–Vis, NIR, Raman, etc ...), type of measurement style (point-by-point, line-by-line or imaging-filter based), required speed, resolution, etc. [18]. The NIR-Hyperspectral image of this work was obtained with a spectrometer (Headwall photonics model 1002A-00371) working in the wavelength range of 1009–1694 nm with a spectral resolution of 4.85 nm (a total of 142 bands were recorded for each spectrum). The camera was placed in right angle respect to the sample. The sample was illuminated with diffuse white light in an angle of 45° respect to the sample. The spectrometer was adapted to a line mapping configuration with a line of 320 pixels. The spatial

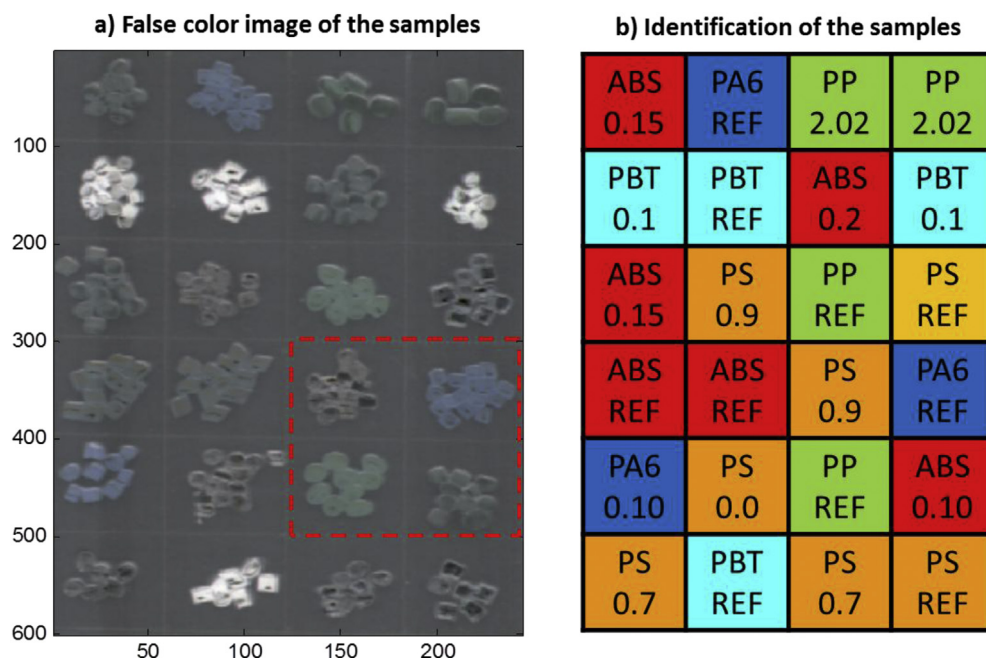


Fig. 1. a) False color image of the pellets of the different plastics measured. The real color was as follow: ABS, PS, PP, black pellets. PBT was transparent. PA6 was brownish transparent. The dashed red square indicates the part of the image used in Sections 4 and 5. b) The identification of each group and sub-groups of plastics. The numbers are only for indication of groups and sub-groups and they should not be taken as any quantity. (For interpretation of the references to colour in this figure legend, the reader is referred to the web version of this article.)

Table 1

Plastic types, main category and sub-categories. The number 2 between parenthesis indicates that there are 2 clusters of the same plastic in the image (see Fig. 1b).

Plastic type	Main category	Sub-categories
Butadiene Styrene	ABS	REF (2); 0.1; 0.15 (2); 0.2
Polyamide 6	PA6	REF (2); 0.1
Polybutylene terephthalate	PBT	REF (2); 0.1 (2)
Polypropylene	PP	REF (2); 2.2 (2)
Polystyrene	PS	REF (2); 0.0; 0.7 (2); 0.9 (2)

resolution can be tuned between 25 μm and 300 μm . In this case, the final pixel resolution was 300 μm . The final image was reconstituted with the aid of CameraLink 14-bit encoding system implemented in the software of the camera. This hyperspectral camera was kindly provided by FOSS (FOSS A/S, Denmark). The spectra were recorded in the reflectance mode.

The calibration of the camera is an essential step that strongly depends on the type of spectral radiation and the setup of the detectors. Always make sure of performing a proper calibration of the camera. In this case, the camera was calibrated using a spectralon plate. If the correction of the hypercube with the reference and dark current is performed automatically by the software, be sure that is performed correctly [64–66].

3.3. Software

Use the most adequate software for your needs. If you have programming skills, the usage of open source software [67,68] can be advisable, in which is very common to find libraries for hyperspectral analysis. The same fact occurs with Matlab [69]. Despite Matlab is not open source, it allows programming and using external toolboxes like, e.g. MIA toolbox [70]. If, on the contrary, you want to keep yourself away from programming, software like ENVI [71], for example, will help you. There are also some other software packages available that are free. But no matter which

software you use, be always aware of how the different multivariate methods are implemented. When you use open code software, this is not much problem. You use your own libraries or you can check what other researchers have programmed. This, though, is more difficult to check in commercial software (see Ref. [72] for an example).

In this case, the hyperspectral image data processing was performed by using HYPER-Tools, an in-house library working under Matlab [69] and freely available upon request (jmar@life.ku.dk for last version). Classification models were performed by using Partial Least Squares-Discriminant Analysis (PLS-DA) implemented in the PLS_Toolbox [73]. Moreover, the image processing methods used in the last section were applied using the Image Processing toolbox [74]. This seems a very complicated combination of software. Nevertheless, the three of them (HYPER-Tools, PLS_Toolbox and Image processing toolbox) work under Matlab environment, and all their utilities can be used in an automatic manner by means of in house-generated scripts.

4. Structure of hyperspectral images

The final result of measuring a hyperspectral image is a 3-D dataset, known as a spectral hypercube (Fig. 2, top left). In the structure of the 3-D dataset \mathbf{X} ($M \times N \times \lambda$), the M and N axes represent spatial information, while λ represents the spectral dimension. This section of the hypercube contains four different plastics (PS, PA6, PP and ABS) and background.

This data structure usually comprises thousands of spectra (spectral signature) distributed over the measured area (spatial signature). Therefore, understanding the structure of your hyperspectral image is essential to select the proper tools for dealing with the final aim. It has not to forget that both spectral and spatial signatures contain the interesting analytical information and, at the same time, different issues that must be handled in a particular and tailored manner. Moreover, both signatures are inherently linked to

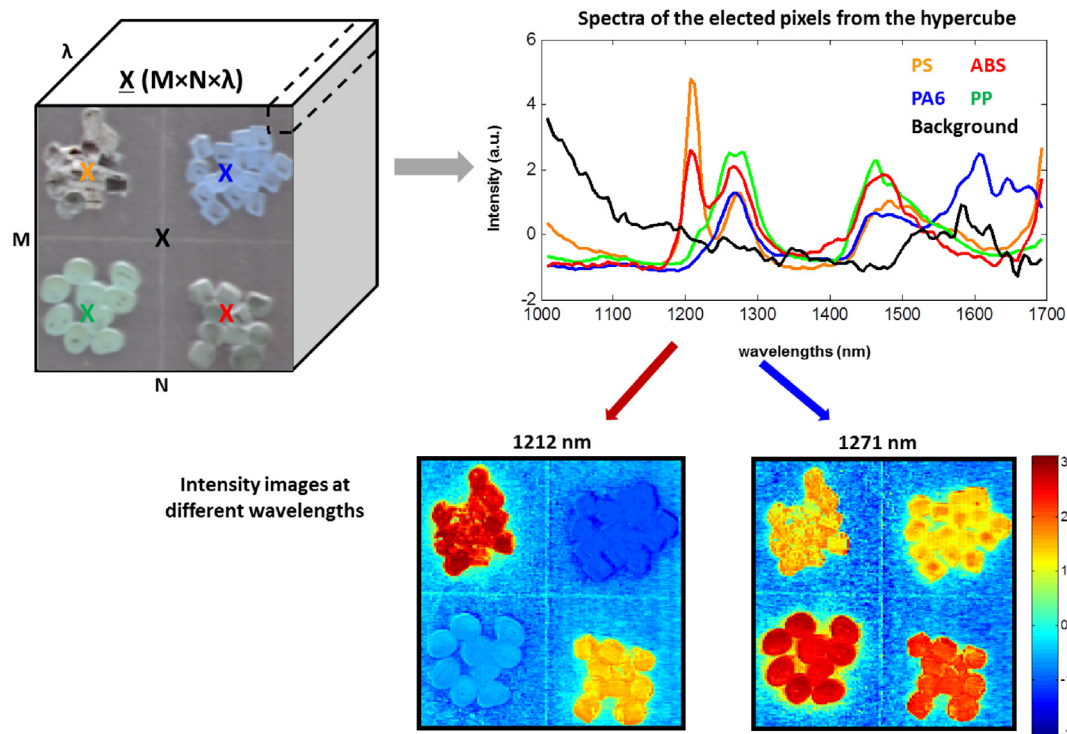


Fig. 2. Structure of a hypercube. Top left: Depiction of a hypercube obtained for the plastics. Several pixels belonging to different plastics plus the background are selected (Orange, PS; Blue, PA6; Green, PP; Red, ABS; Black, background) and their corresponding spectral profile shown in the top right figure. The bottom figure represents the hyperspectral image obtained for two different wavelengths (intensity/false color images) without the influence of the background. (For interpretation of the references to colour in this figure legend, the reader is referred to the web version of this article.)

each other. That is, the spatial distribution of a specific compound will be fully assessed if the spectral signature of the same compound is selective enough to be independently extracted from the rest, and vice versa. Assessing the spatial distribution of elements in one surface (e.g. studying homogeneity or distribution of elements) is not an easy task and is far out from the scope of this manuscript. Therefore, more emphasis will be given in defining the characteristics of the spectral signature.

Each pixel represents a spectrum that is the sum of the absorbances/influences/counts of all the compounds ($k = 1 \dots K$) present in that particular pixel plus the unavoidable spectral noise. Taking NIR as example, the absorbance for a single pixel mn at one wavelength λ can be postulated as:

$$a_{mn\lambda} = \varepsilon_{\lambda 1} C_{1mn} + \varepsilon_{\lambda 2} C_{2mn} + \dots + \varepsilon_{\lambda k} C_{kmn} + e_{mn\lambda} \quad (1)$$

where ε is a constant that depends on the respective wavelength, C is the concentration of the k th absorbing compound in the specific sample, and e is the noise. This equation can be generalized for every single pixel in all wavelengths (Equation (2)), where \sum represents the so-called pure spectrum of a specific compound.

$$a_{mn} = \sum_1 C_{1mn} + \sum_2 C_{2mn} + \dots + \sum_k C_{kmn} + e_{mn} \quad (2)$$

It is important to note that a single pixel should not be treated as a single sample. It is, indeed, strongly influenced by different issues:

- Irregularities and shape of the surface: the surfaces measured with hyperspectral cameras are seldom totally flat. This, of course, depends on the final resolution of the image. Simple examples of this idea are the roughness of a tablet or the shape of an orange. This affects the light intensity that one pixel

receives and, therefore, the light intensity that is reflected and arrives to the detector.

- Penetration depth of the electromagnetic radiation: Most of the spectral radiation collected by the detector concerns to the surface of one sample. Nevertheless, vibrational spectroscopy has certain penetration depth [75]. This makes that a pixel usually contains not only information of the surface layer of the sample, but also of the most adjacent internal layers, as well as the adjacent pixels.
- Resolution: It is seldom found that a pixel contains selective information of one component. For example, tablets are usually measured with a pixel resolution that is bigger than the particles sizes. Therefore, a pixel will contain mixed information of all the components present on it.

5. General scheme to perform hyperspectral image analysis

Due to the fact that the obtained spectra seldom contain selective wavelengths for a specific compound, and that a pixel usually contains mixed information of more than one compound, the use of multivariate data analysis has become an essential keystone of the hyperspectral image analysis. Chemometrics is currently a very well-known discipline that has been used for many years on hyperspectral images as well. This has generated that, depending on the purpose, different procedures can be chosen. A general, but not exclusive, flow-chart is depicted in Fig. 3.

The main building blocks of Fig. 3 are: 1) Spatial and spectral pre-processing, 2) exploration, 3) resolution and/or regression, 4) segmentation and 5) final image processing. Every step has been widely defined in several reviews [5–8,18], giving a comprehensive explanation of every step and several applications. As mentioned in

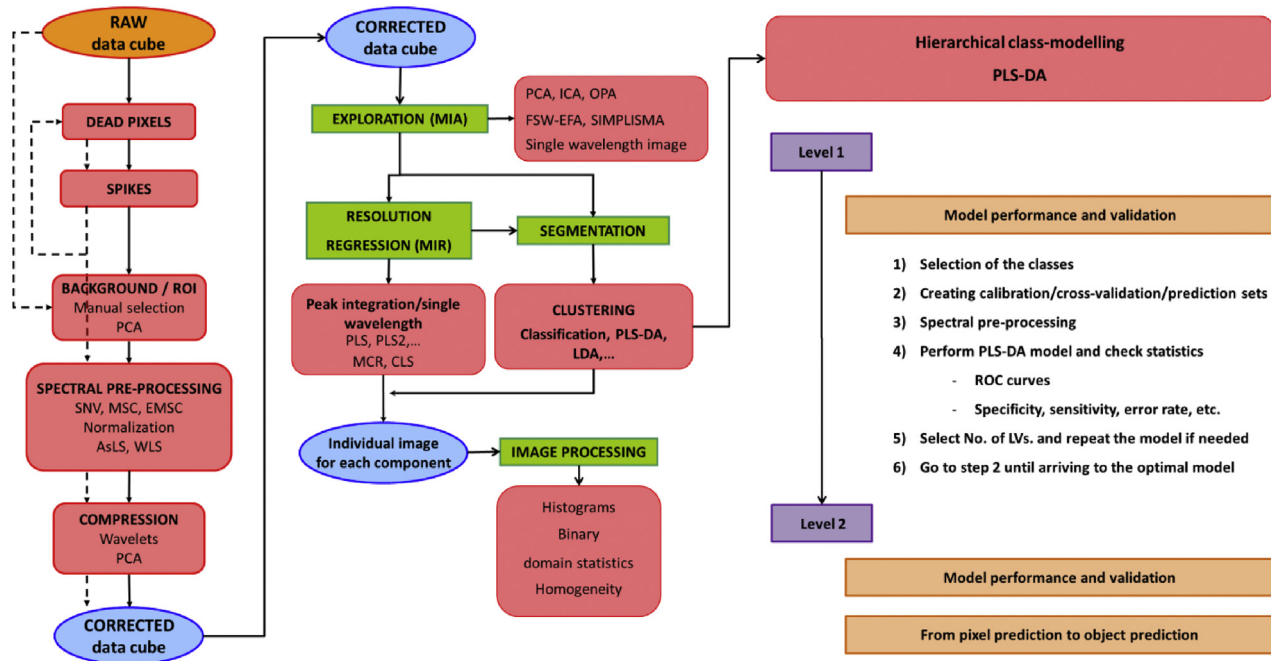


Fig. 3. Comprehensive flow-chart for the analysis of hyperspectral images. Partially extracted and modified from Ref. [18] with permission of Elsevier.

the introduction, Sections 6–8 will deepen in the development of classification models for the different plastic categories plus the final image processing step. Important parts of hyperspectral image analysis like exploration and resolution/regression will not be explained in those sections. Instead, they will be exemplified herein, together with further information of spatial and spectral pre-processing, taking the small portion of the hypercube in Fig. 2 as example.

- Spatial pre-processing: Usually, this part is linked to the selection of the Regions Of Interest (ROIs) in the image, also referred to as masking the non-interesting areas. Since eliminating the unwanted pixels is not physically possible (otherwise the 3D structure would be lost), the most common procedure is creating a mask, with the same spatial dimensions than the image, but containing information for every single pixel concerning its selection for subsequent analysis. In Matlab's language, this mask is a logical matrix containing 0's and 1's, denoting no-selection and selection, respectively.

There are many different methods to perform masking (e.g. Principal Component Analysis, selective wavelength selections, clustering, etc). When to use one or another will strongly depend on the spectral signal of both the background and the elements in the image. Therefore, it is also common to perform spectral pre-processing in order to highlight the differences between the background and the objects of interest. As an example, Fig. 4 shows a flowchart to eliminate the background using K-means clustering. Since sometimes is difficult to guess the amount of clusters needed to collect all the plastics, K-means was performed by using 2 and 4 clusters to the spectra pre-processed with first derivative. As it can be observed, all plastics are perfectly collected in cluster 1 if two clusters are calculated. Nevertheless, it might be the case that more clusters are needed. If 4 clusters are calculated, for instance, clusters 1 and 2 can be selected as the ones belonging to the ROI (white areas in the rightmost pictures). The rest of the pixels (black areas) will be discarded for further analysis.

- Spectral pre-processing: Spectral pre-processing aims at both avoiding the influence of undesirable phenomena coming from the measurement (like light scattering or spectral noise), and highlighting the differences between spectra for subsequent analysis. This has been done so far by the adaptation of the pre-processing techniques applied in classical spectroscopy. The first artifact to be removed is the influence of the instrumental noise in the spectra. Methods for smoothing or de-noising have been proposed, among which Savitzky-Golay method is one of the most accepted [76]. Apart from the instrumental noise, the different spectral artifacts that spectra can present strongly depend on the type of the radiation. For instance, NIR radiation is usually affected by light scattering. Therefore, methods like Standard Normal Variate (SNV) or Multiplicative Scatter Correction (MSC) are commonly used to minimize this effect [76]. Looking at Fig. 5 it can be observed how the difference between the plastics at wavelength 1212 nm becomes more relevant when the scattering is minimized by using SNV (Fig. 5b) respect to the image obtained using the raw spectra (Fig. 5a).

Raman spectroscopy, on the contrary, is usually affected by the fluorescence interference, having many different methods for baseline modeling [77,78]. A particular case of spectral pre-processing is the use of derivatives. First and second order derivatives help to minimize the spectral noise, suppress spectral artifacts, and to highlight the differences between the spectra (Fig. 5c).

Despite the benefits that different pre-processing methods offer, they must be applied with care, since a wrong selection of the pre-processing method may distort the useful information of the spectra. This is the case of the application of the derivatives with Savitzky-Golay filters. First, the derivatives change the shape of the spectra, making more difficult their interpretation. Second, the selection of the proper window for fitting the polynomial plays a fundamental role. Choosing small windows may generate noise in the spectra; whereas the selection of a wide window may eliminate important information if the spectra contain sharp peaks.

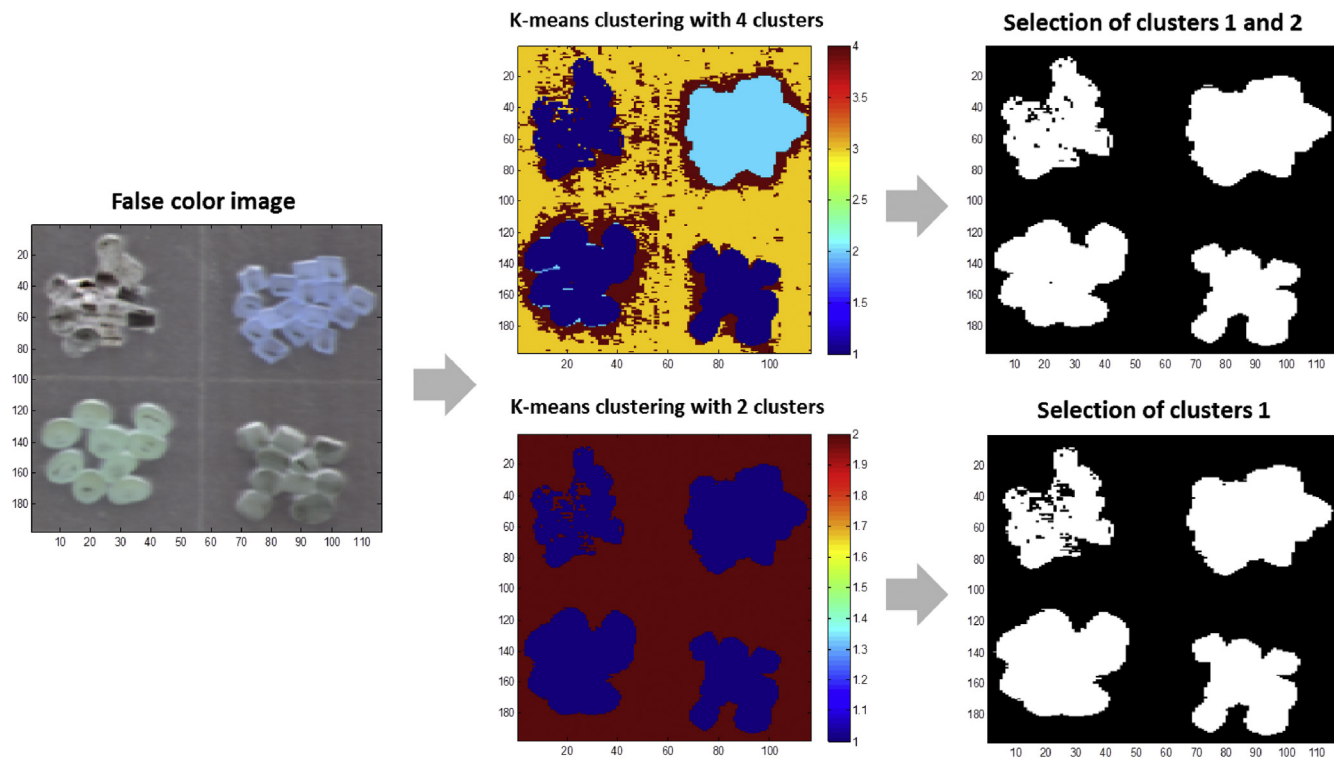


Fig. 4. Masking of the selected area of the hypercube by using K-means clustering calculated with 4 and 2 clusters.

- **Multivariate exploration of images:** Among all the methods that can be found in the literature for multivariate exploration, Principal Component Analysis (PCA) is the most versatile and useful [18]. As it is well known, PCA aims at studying the variability (variance) of the surface under study, dividing the hypercube into a set of surface scores and spectral loadings [5,10,18]. It is wrongly believed that every score surface obtained should correspond to one single compound. This is not always true, since PCA looks for variance. To exemplify this point, a PCA model of the small hypercube (Fig. 2) is shown in Fig. 6. This PCA model was performed with the spectra in first derivative and mean centered. The total amount of variance explained by the first and second principal components (PC1 and PC2, respectively) was higher than 83%, denoting that the main differences between the plastics are within these two PCs, if no other artifact is present in the surface (e.g., light scattering).

What is interesting from this PCA model is that the four classes of plastics can somehow be differentiated each other by only using two PCs. Looking at the score surface and the corresponding loading of PC1 (Fig. 6a and b, respectively), it is clear that this PC explains the main difference between PA6 and the rest of the plastics. The correspondence between the negative part of the score surface and the loading suggests that the main source of difference for PA6 is located in the last wavelength range (1500–1700 nm). Analogously, PC2 (Fig. 6c and d) grades the other three plastics in intensity depending of the influence of a main peak located around 1200 nm and the two peaks in its positive part. Here, it is important to remark that PCA is not a classification model. With PCA we can only study the variance and have some clues of the actual classification method that will be applied afterwards.

- **Multivariate resolution of images:** Curve resolution methods also decompose the hypercube into a set of score surfaces and

loadings, as PCA does. The main and crucial difference is that the scores and loadings obtained with curve resolution methods are calculated in such a way that they do not maximize the variance of the hypercube, but extract the real physicochemical behavior of all the components in the surface studied. That is why the scores and loadings are usually called relative concentration surfaces and pure spectra, respectively. Accordingly, in the example proposed, it would be expected to obtain one concentration surface and one pure spectrum for each class of plastic. The main tool for performing curve resolution is the so-called Multivariate Curve Resolution (MCR) method [79,80]. MCR is an extremely versatile curve resolution method that has been applied on hyperspectral images for several years now in many different fields [5,7,8,16,18,81–86]. Nevertheless, despite the attractiveness of a method that is able to recover the real chemical behavior of the components in a surface, it must be highlighted that sometimes arriving to the proper solution is cumbersome and requires the addition of extra information and proper constraints to the model. In this respect, de Juan and co-workers have a great experience applying MCR and showing how to properly apply MCR [82–88] and the reading of the recommended references is highly advisable for researchers who want to perform MCR models in their images.

6. Classification model development for the five major categories of plastics

As said before, this manuscript will focus on classification methods. Specifically, the application of a class-modeling method, like Partial Least Squares-Discriminant Analysis (PLS-DA) in a hierarchical manner (Fig. 7), will be discussed. The hierarchy of the models will be based on two steps:

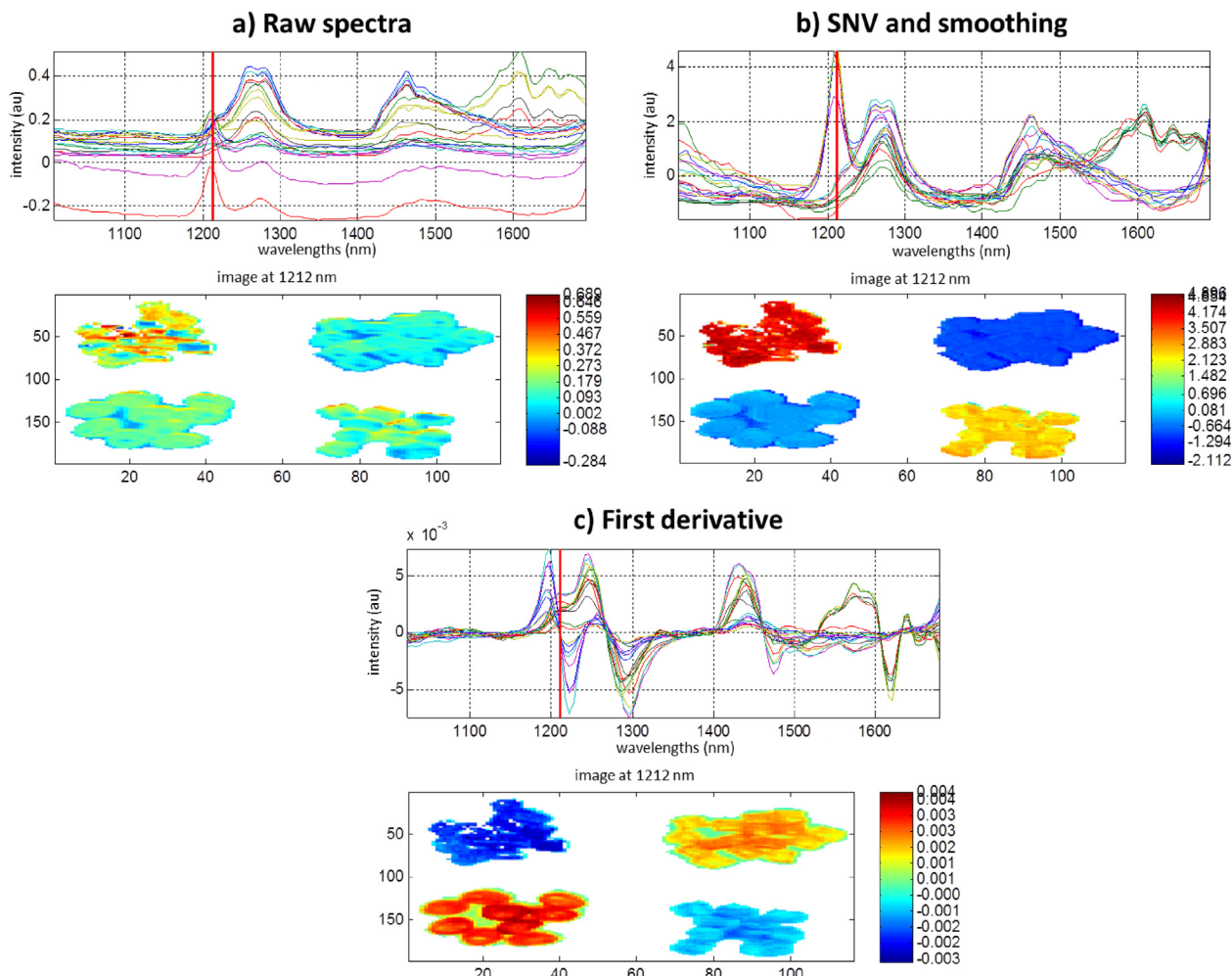


Fig. 5. Influence of different spectral pre-processing methods on the spectra of the hypercube included in the analysis. a) raw spectra, b) Pre-processed spectra with SNV and smoothing (Savitzky-Golay with a window size of 7 and second order polynomial degree), c) First derivative spectra (Savitzky-Golay with a window size of 7, second order polynomial degree and first order derivative degree).

- 1) The plastics will be separated according to their different composition of the main class.
- 2) The second step involves the creation of individual models for each plastic to discriminate between plastics containing flame retardant.

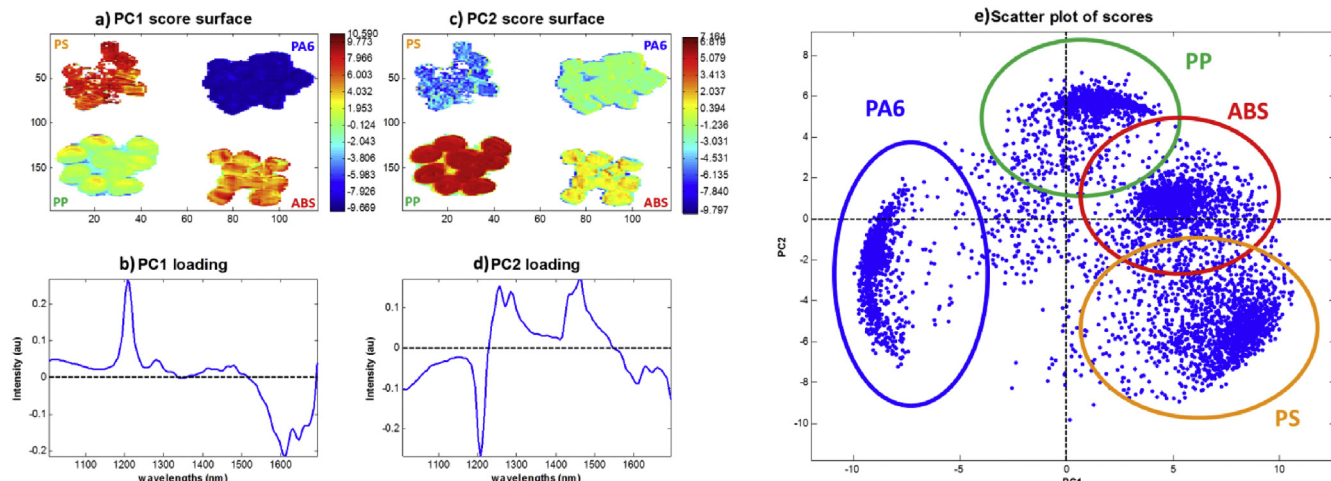


Fig. 6. PCA model of the hypercube. a) Score surface and b) corresponding loading of PC1. c) Score surface and d) corresponding loading of PC2. e) Scatter plot between PC1 and PC2 scores. Every dot corresponds to one pixel.

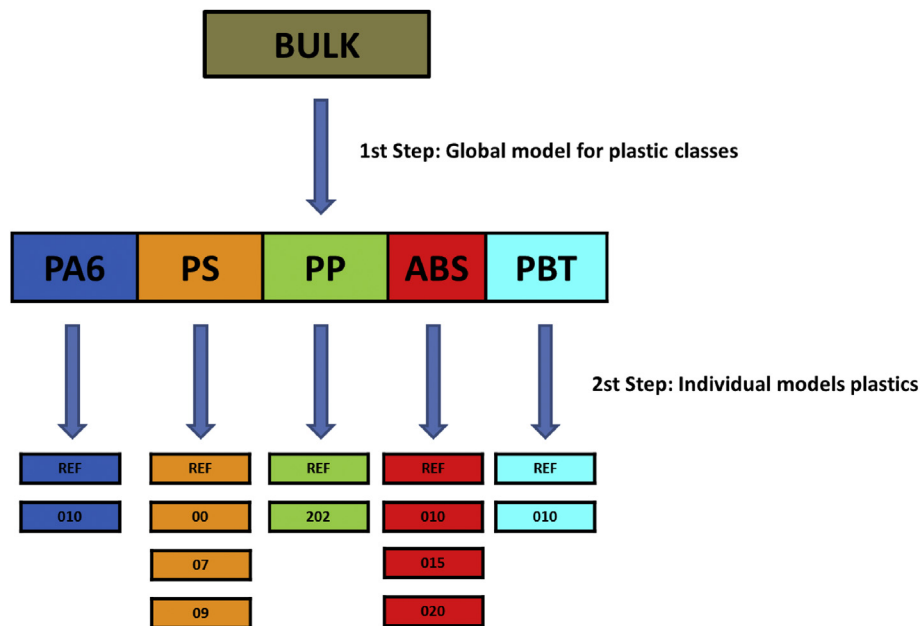


Fig. 7. Two steps strategy for plastic sorting. The different categories are defined in material and methods section.

6.1. Hypercube pre-processing

Following the scheme on Fig. 3, the first step is to remove the background. The method chosen in this case to generate the mask

was K-means clustering (two clusters) applied on the derivative spectra, as explained before. For the subsequent classification model, the spectra chosen by the masking process were subsequently pre-processed by using Standard Normal Variate (SNV) [76]

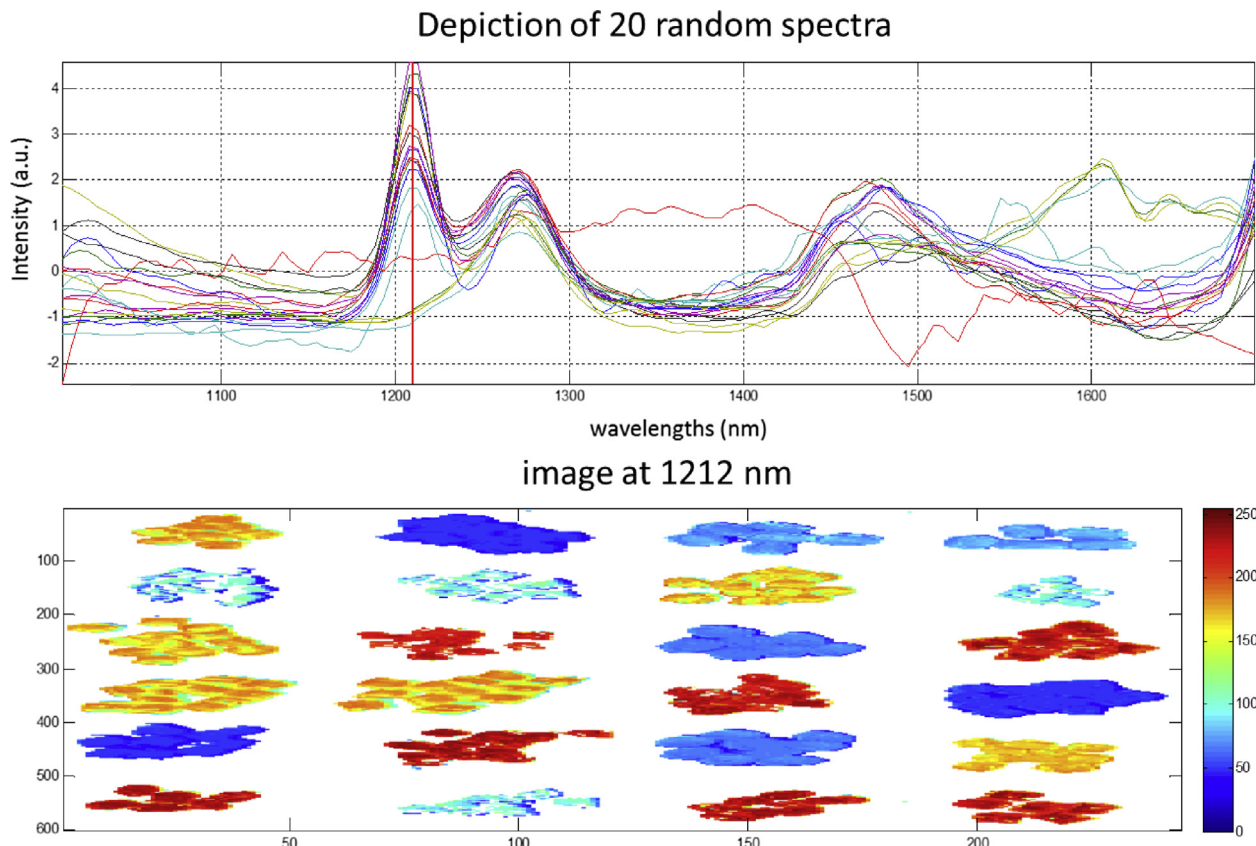


Fig. 8. Top, 20 random spectra of the pre-processed image. Bottom, normalized false color image taken at 1207 nm. (For interpretation of the references to colour in this figure legend, the reader is referred to the web version of this article.)

and smoothing (Savitzky -Golay filter with window size of 7 points and second degree polynomia). The final pre-processed spectra are shown in Fig. 8.

After de-noising and/or highlighting the spectral information, the spectra must be normalized prior to carry out any multivariate analysis to leverage the importance of all the spectral variables. Therefore, the final procedure (and almost mandatory when continuous spectra are measured) is the application of mean centering of the spectra [52].

Observing carefully the selected ROIs in the image generated at 1212 nm (Fig. 8, bottom) it can be noticed that there are still pixels that belong to the background within several pellets. These pixels are sometimes hard to eliminate. This is the problem when objects are close each other or even touching. The different spectra of the objects affect the spectra of the background nearby the objects, making the task of background removal quite complex if an automated method is applied. For now, we will keep those pixels in the analysis, since it is interesting to see how the classification model handles them. In Section 8 we will remove them and evaluate the difference.

6.2. PLS-DA model performance

Once the spectra are properly pre-processed and normalized, the first classification model was developed by only considering the 5 major categories: ABS, PS, PA6, PP and PBT. PLS-DA [89] is a supervised class-modeling method that uses the PLS algorithm to predict the belonging of a sample to a specific class. Therefore, to create the calibration model, a **X** matrix containing the spectra for calibration, and the corresponding **Y** matrix containing the belonging identity for each class, is needed. The **X** matrix can be generated from standard images of the plastics, after an unfolding step (as shown in Fig. 9) [18,81], or, as in this case, by selecting a percentage of the pixels from the image. It is wrongly thought that PLS-DA models can only be performed when two classes need to be classified. In a multi-class task, PLS-DA models are usually performed by using PLS2 algorithm. Therefore, the **Y** matrix will have as many columns as classes, and as many rows as pixels/spectra used for the calibration. This is called the dummy matrix, and it only contains 1's and 0's, indicating the belonging or not belonging

to one spectrum to a specific class, respectively (Fig. 9).

Due to the high amount of pixels (an inherent advantage of images), 65% of them, randomly selected for each class, were used to build the model. As a matter of fact, it never hurts to remember that all multivariate models developed for classification and regression must be validated. Validation is the main tool that tells us how our model predicts, since a good model is not the one that better calibrates, but better predicts. Usually, cross-validation is the correct choice. But profiting the great amount of pixels in hyperspectral images, it is worth implementing a validation with an external set of pixels that have not been used for model development. Thus, this model was validated by using cross-validation (random subsets cross-validation approach) and using the rest of the pixels as external test set (the 40% of the pixels not used to develop the model).

The model will predict the response of the classes based on PLS2. Consequently, the results will not be either a 1 or a 0 perfectly, then a threshold must be set in the predictions. There are many ways of setting this threshold, among which the application of the Bayes Theorem is one of the most accepted ones. Assuming that the predictions between 0 and 1 follow a normal distribution, the threshold is established in the **y** value at which the number of false positives and false negatives is minimized (see Section 6.3).

Another important step is the selection of the proper number of latent variables (LVs). It is a choice to use the evolution of the Root Mean Square Error (RMSE) with the number of LVs. RMSE is calculated based on the actual predicted values between 0 and 1 (e.g. 0.3, 1.2 or -0.2). This is valid for regression models. Nevertheless, when classification is performed, every sample is directly associated to one class. Hence, checking the evolution of the classification error (class error, see Section 6.3) for calibration, cross-validation and external test set with the number of LVs is preferred.

The results, as expected, were of high quality in terms of classification performance. In Fig. 10a it is very easy to recognize that the 5 plastics have been perfectly separated in the score space spanned by the first 3 LVs space.

One aspect that usually is not thoughtfully investigated is the extremely rich information that loadings offer (Fig. 10b). Indeed, they allow us to understand the real reason of the separation of the plastics. Observing them, together with the score plot, can give an

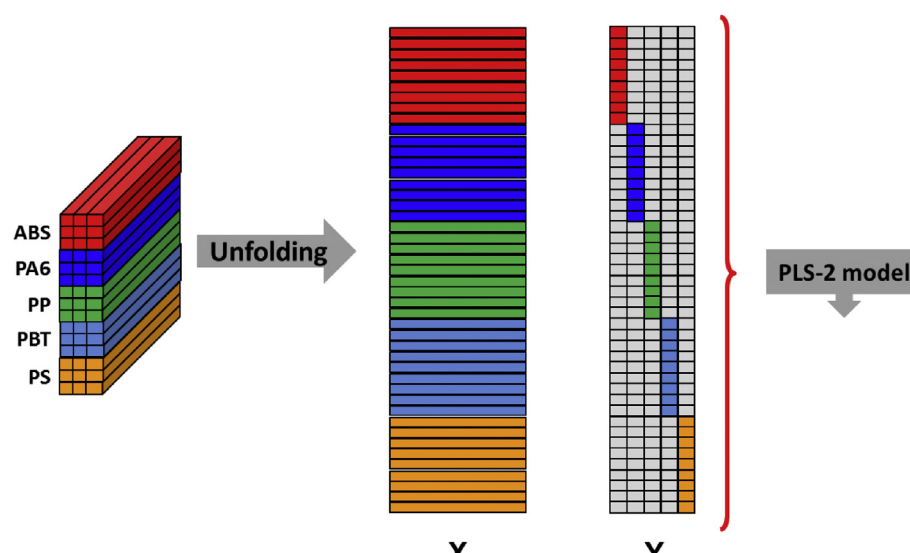


Fig. 9. Arrangement of the **X** and **Y** matrices for developing the PLS-DA classification model. In the **Y** dummy matrix, the grey areas contain 0's, while the colored areas contain 1's. (For interpretation of the references to colour in this figure legend, the reader is referred to the web version of this article.)

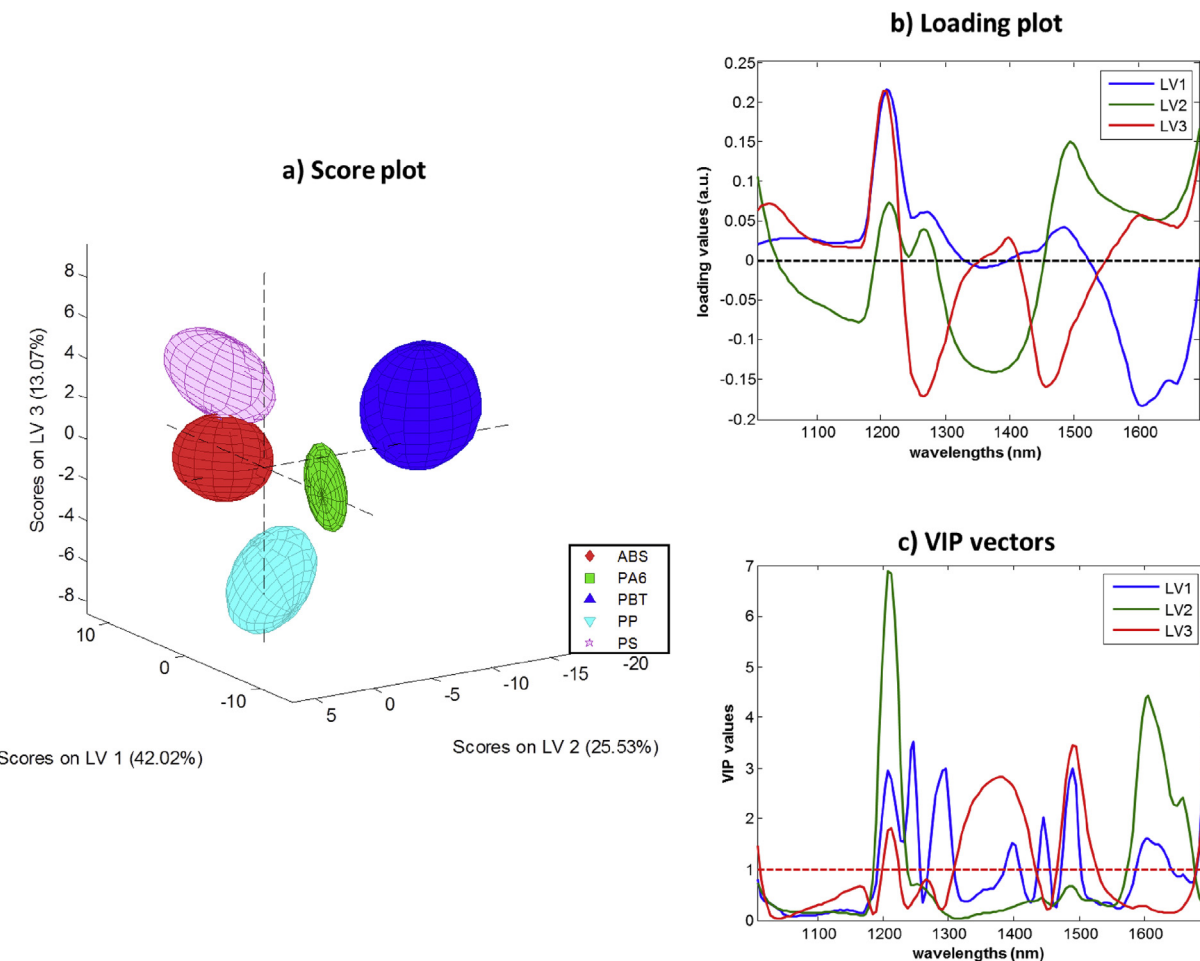


Fig. 10. a) Scores, b) loadings and c) VIP vectors plots of the general PLS-DA model.

idea of which variables are the most important ones in the separation of the classes. Moreover, every time a targeted multivariate model is developed, there will be the option of performing variable selection for improving the models. It is also worth exploring some methods which assess the variables responsible for the separation of the groups in a more statistical manner. In this case, the software used contains the Variable Importance in Projection (VIP) score for the loadings [90], denoting that variables with a VIP value higher than one are the ones responsible for the classification (Fig. 10c).

6.3. Statistical assessment of the model

The statistical assessment of the classification performance can be done by using different classifiers [91–93]. In our case, the model was statistically validated by using the sensitivity, specificity and class error for the calibration (CAL), cross-validation (CV) and external test set (PRED):

$$\text{Sensitivity} = \frac{TP}{TP + FN} \quad (3)$$

$$\text{Specificity} = \frac{TN}{FP + TN} \quad (4)$$

$$\text{Class error} = 1 - \left(\frac{\text{Sensitivity} + \text{Specificity}}{2} \right) \quad (5)$$

In the equations, TP and TN stand for true positive and true negative, respectively, accounting for the pixels that have been correctly assigned as belonging (TP), or not belonging (TN), to a specific class. FP and FN stand for false positive and false negative, respectively, accounting for the pixels that have been wrongly assigned as belonging (FP), or not belonging (FN), to a specific class.

The statistical results are, indeed, very impressive (Table 2). The first point to observe is the high similarity between the values obtained for calibration, cross-validation and external prediction. This indicates that the models are not under or over-fitted. Apart from that, the sensitivity and specificity values obtained for every single plastic in external prediction were greater than 0.95 (except the sensitivity of PA6). That means that there is a probability higher than 95% of classifying correctly every single pixel in its corresponding category.

Another important statistics often used in classification is the Receiver Operator Characteristics (ROC) curves. The ROC curves are graphical plots that illustrate the performance of the classification as its discrimination threshold (relationship between the specificity and sensitivity) is varied. For the external test set, the ROC curves obtained are observed in Fig. 11. In this figure, the red dot indicates the threshold obtained for the external test set. This threshold must be, as in this case, as close as possible to the one obtained for the calibration and cross-validation sets.

Regarding the pixels within pellets, it is remarkable to see how most of them have been assigned to belong to the corresponding plastic (Fig. 12). This may lead to problems in terms of accuracy of

Table 2

Sensitivity, specificity ad classification error for the five main categories of plastics.

	Global model				
	PA6	PBT	PP	PS	ABS
Sensitivity (CAL)	0.945	0.993	0.964	0.991	0.985
Sensitivity (CV)	0.946	0.993	0.963	0.991	0.983
Sensitivity (PRED)	0.864	0.996	0.967	0.983	0.972
Specificity (CAL)	0.964	0.997	0.976	0.998	0.979
Specificity (CV)	0.965	0.997	0.976	0.998	0.979
Specificity (PRED)	0.957	0.995	0.96	0.993	0.962
Class error (CAL)	0.044	0.004	0.03	0.005	0.018
Class error (CV)	0.044	0.005	0.03	0.005	0.019
Class error (PRED)	0.089	0.004	0.036	0.011	0.032

the model, since those pixels belong to the background.

Fig. 12 also shows that a small portion of the pixels have been unassigned (deep blue pixels in Fig. 12). This might be due to two reasons: the known fact that there are pixels belonging to the background that have not been eliminated; and the different surface characteristics of the plastic pellets, which are not completely flat. This points out that despite the pre-processing steps, total suppression of artifacts coming from the roughness and the shape of the surfaces is not always possible.

7. Classification models for each individual category

Once every plastic class has been separated from the rest, the second step is the development of individual PLS-DA models for

every category to classify the plastics according to their content of flame retardant. Different number of LVs and different spectral pre-processing methods were needed in order to obtain optimal results. This was tested with the same validation procedure as before: cross-validation based on random subsets selection and external test prediction. The parameters for each plastic and the optimal number of LVs are shown in Table 3.

The statistic results for the classification parameters are shown in Table 4. This table clearly shows that PA6 and PP can be successfully separated from the corresponding plastics containing flame retardant. Acceptable results were also obtained for PBT, ABS and PS, but not as good as the ones obtained with PA6 and PP.

Looking at the prediction results of the image (Fig. 13), it can be observed that the amount of pixels not classified in their corresponding class for ABS and PS is extremely high. Also, focusing on the ROC curves obtained for ABS (Fig. 14), there is a strong confounding effect within the subclasses.

The reasons for the not totally satisfactory performance of the models for ABS and PS could be: the high similarity between the spectral signature of the sub-classes, the roughness of the pellets, and the presence of pixels belonging to the background.

8. From pixel-wise to object-wise projection

As mentioned beforehand, there are still several background pixels that were not totally eliminated by the automatic mask procedure applied. The elimination of these pixels is sometimes difficult, since the spectral influence of the pellets around the background pixels makes their spectra closely similar to those ones

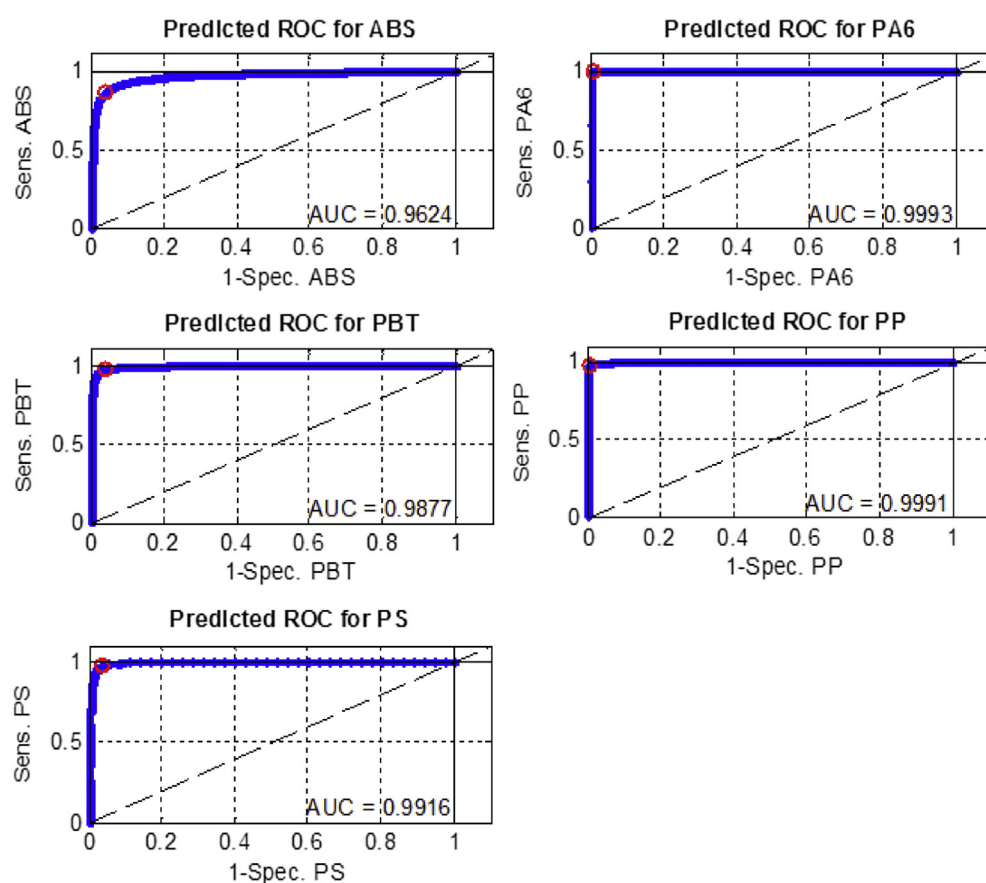


Fig. 11. ROC curves obtained for the external prediction set of the first model. The red dot indicates the threshold obtained for the external test set. (For interpretation of the references to colour in this figure legend, the reader is referred to the web version of this article.)

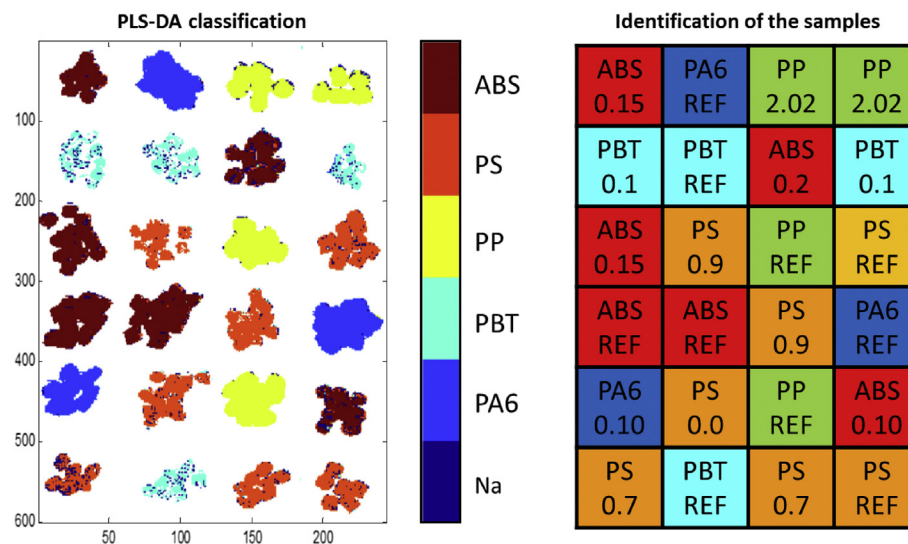


Fig. 12. External prediction of the standard sample to verify the usefulness of the global PLS-DA model (Na stands for “not assigned” pixels).

Table 3

PLS-DA model parameters for every plastic category.

Plastic	LVs	Pre-treatment
ABS	7	SNV + Second derivative
PS	8	SNV + smoothing
PBT	6	SNV + smoothing
PA6	6	SNV + First derivative
PP	8	SNV + smoothing

of the pellets. Moreover, there are pixels belonging to pellets that have not been assigned to any class due to the different physical characteristics of the pellets.

For solving the first issue, we can take advantage of using digital image processing methods, aiming at assigning an identification mark for each pellet, in such a way that all the pixels belonging to those pellets are classified in the same class.

The second issue is more related to the philosophy behind the aim of the separation. In our case, the pellets used are of homogeneous composition. One solution might be to assign the whole pellet to the most contributing class (the class that has the largest number of pixels in that pellet). It should be noted that the solution

makes sense only when the number of pixels assigned to the most contributing class is high, compared to the total number of pixels in the pellet. This condition helps to avoid random assignments of the pellet to a class.

8.1. Suppression of the pixels within the pellets

There are as many methods for digital image processing as you can imagine. A good reference to start learning about some of the most important methods is the book in Ref. [94].

In our case, the first step consists of using an image that represents the shape of the pellets and the contrast with the inner background pixels as good as possible. This can be done by selecting a specific wavelength or the combination of usually three different wavelengths to create a false RGB image. For instance, the false RGB image observed in Fig. 1 was constructed by dividing the whole spectral interval into three equivalent intervals and averaging the absorbance values in each pixel. This image, thought, is not very clear. Therefore, three different wavelengths were chosen from the hyperspectral image with the spectra in first derivative. The chosen wavelengths were 1237, 1295 and 1441 nm, since they were the ones giving the highest contrast between the background and the

Table 4

Sensitivity, specificity and error rate for the PLS-DA models developed for each plastic.

	ABS				PS			
	ABS10	ABS15	ABS02	ABS	PS00	PS07	PS09	PS
Sensitivity (CAL)	0.892	0.87	0.831	0.755	0.931	0.878	0.698	0.81
Sensitivity (CV)	0.891	0.87	0.826	0.752	0.924	0.873	0.693	0.812
Specificity (CAL)	0.57	0.837	0.737	0.635	0.83	0.763	0.65	0.842
Specificity (CV)	0.569	0.837	0.737	0.631	0.83	0.762	0.648	0.841
Class error (CAL)	0.269	0.146	0.215	0.304	0.119	0.179	0.325	0.174
Class error (CV)	0.27	0.146	0.218	0.308	0.122	0.182	0.329	0.173
PBT				PA6		PP		
		PBT010		PA6010	PA6	PP202	PP	
Sensitivity (CAL)	0.807	0.599	0.856	0.893	0.945	0.944	0.944	
Sensitivity (CV)	0.798	0.603	0.852	0.895	0.944	0.945	0.945	
Specificity (CAL)	0.599	0.807	0.893	0.856	0.944	0.945	0.945	
Specificity (CV)	0.603	0.798	0.895	0.852	0.944	0.944	0.944	
Class error (CAL)	0.296	0.296	0.125	0.125	0.055	0.055	0.055	
Class error (CV)	0.299	0.299	0.126	0.126	0.055	0.055	0.055	

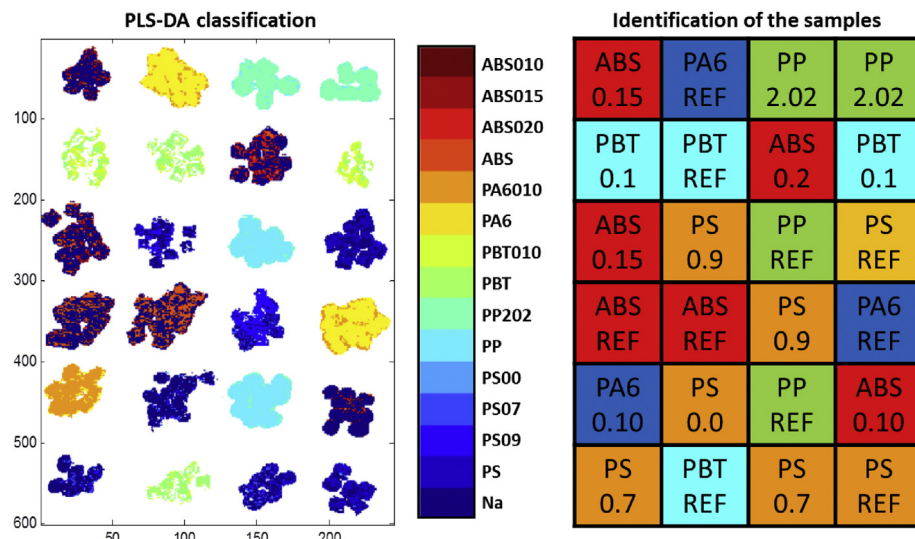


Fig. 13. Cross-validated prediction for every plastic and their corresponding version containing flame-retardant. (Na stands for “not assigned” pixels).

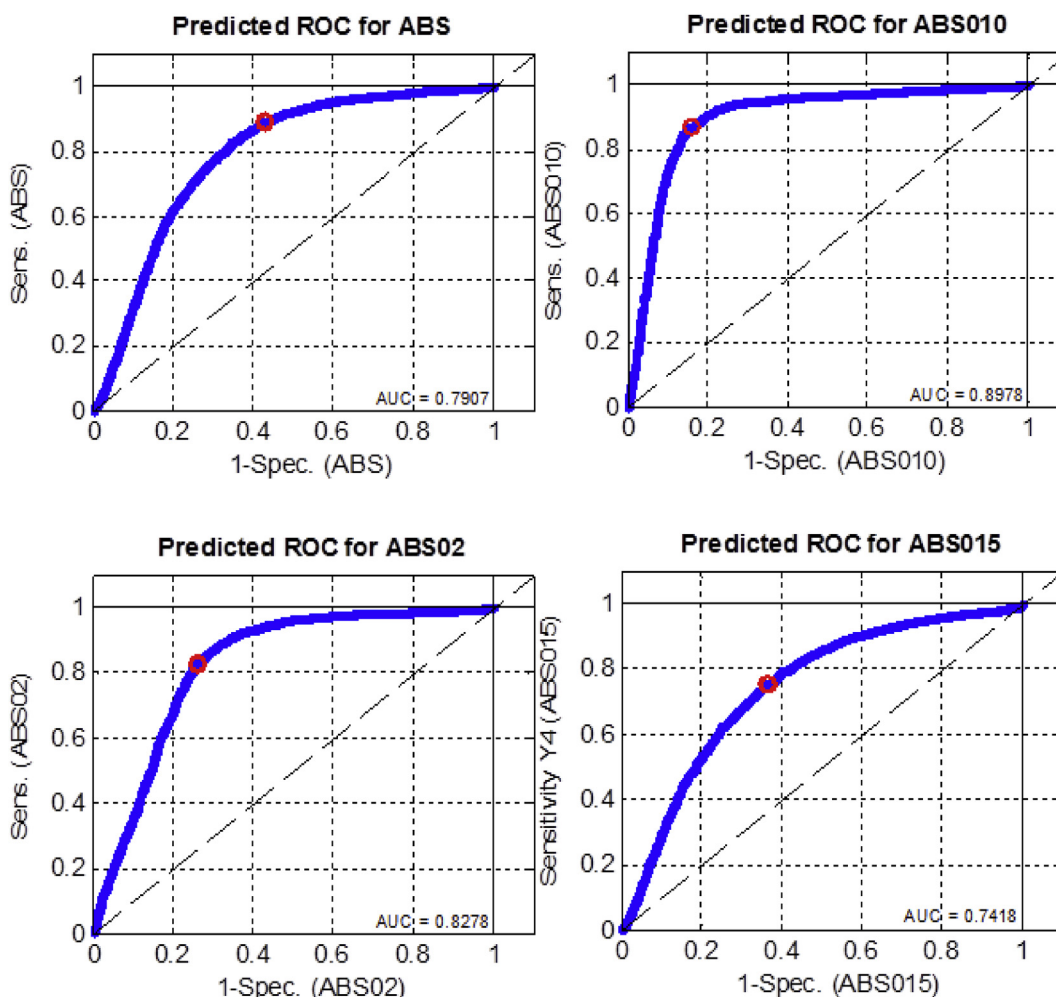


Fig. 14. ROC curves obtained for the external prediction set of the first model. The red dot indicates the threshold obtained for the external test set. (For interpretation of the references to colour in this figure legend, the reader is referred to the web version of this article.)

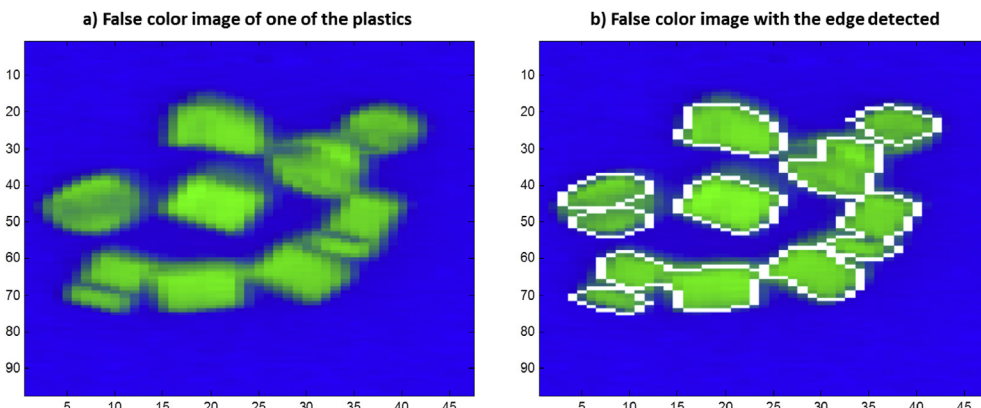


Fig. 15. a) False RGB image created by the combination of the images obtained at three different wavelengths and b) the segmentation of the pellets with the contour in white.

pellets. A small region of the final false RGB picture can be seen in Fig. 15.

This region of the original image has been chosen because almost all the pellets are touching each other, and this represents a problem. There are many ways to tackle this problem. The one represented here is one of the options:

- 1) Transform the RGB image into a grayscale image.
- 2) Image adjustment of the color maps in such a way that the values between 0.4 and 1 (in intensity of the corresponding RGB color map) map to values between 1 and 0.4, respectively.
- 3) Edge detection by using the Laplacian of Gaussian method [95].

The final result is shown in Fig. 15b. As it can be observed, the contour obtained for each pellet allows us to identify each individual pellet in most of the cases. Moreover, the pixels belonging to the background have been totally removed. Nevertheless, there are still some pellets that cannot be separated and, what is more important, one pellet has been split into two. Of course, this can be solved by a manual intervention on the image. However, the point is to show that even when robust methods exist, they must be optimized for every case and sometimes it is difficult to find a "perfect" solution.

8.2. PLS-DA results projected to the individual pellets

This methodology was applied to the whole image and, as defined before, every pellet obtained was treated as an individual for classification. The results of the application of the hierarchical model can be seen in Fig. 16.

With the aim of showing another very practical tool in classification, Table 5 shows the confusion matrix obtained in cross-validation (in this case, no external set was prepared, since the number of pellets for each class is not very large). The confusion matrix gives information of which pellets have been correctly classified (numbers in green in the table) and which ones have been misclassified (numbers in red in the table). Analogously to what happened previously, there are some pellets in the ABS and in the PS classes that have been misclassified within the corresponding sub-class. Moreover, there are also some pellets in PBT010 that have been classified as pure PBT.

9. Remarks and final comments

This tutorial gives some ideas of how to deal with several issues concerning the development of classification models in

hyperspectral imaging in a practical and visual manner. In addition, key references and some hints of very fundamental aspects dealing with hyperspectral image analysis are provided. As stated at the beginning, every single case needs a tailored solution. Therefore, the methods employed in every step must be taken as an optimal solution for this particular case.

Going through the results obtained, all the pellets were correctly classified between the different main categories of plastics. Nevertheless, there are still some issues regarding the classification of the pellets within the classes with and without flame retardant. This is mainly due to the lack of difference between the pellets of the same plastic, but with different amount of flame retardant. From a more applied point of view, the methodology proposed can be easily implemented in a company for plastic sorting, since all the methods used herein can be easily automatized. Of course, there is always room for improvement. To improve the classification results, the first action would comprise a better separation of the pellets in a, for instance, a conveyor belt. The second action would concern looking for increasing the wavelength range. Nowadays is

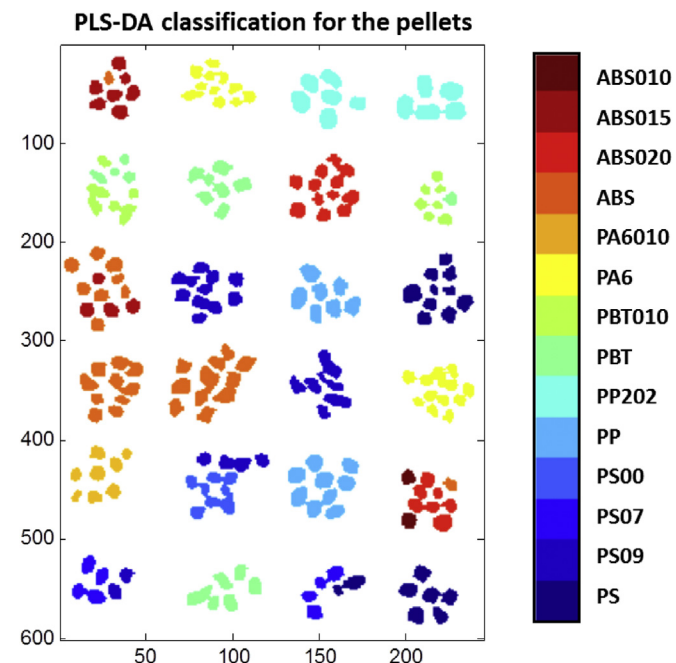


Fig. 16. PLS-DA classification results for the image considering the pellets as samples.

Table 5

Confusion matrix obtained for the PLS-DA model applied to the single pellets. Misclassified pellets in red and correctly classified pellets in green.

		Predicted class													
		ABS010	ABS015	ABS020	ABS	PA6010	PA6	PBT010	PBT	PP202	PP	PS00	PS07	PS09	PS
Real class	ABS010	2	0	7	1	0	0	0	0	0	0	0	0	0	0
	ABS015	0	11	0	9	0	0	0	0	0	0	0	0	0	0
	ABS020	0	0	12	0	0	0	0	0	0	0	0	0	0	0
	ABS	0	0	0	21	0	0	0	0	0	0	0	0	0	0
	PA6010	0	0	0	0	8	0	0	0	0	0	0	0	0	0
	PA6	0	0	0	0	0	22	0	0	0	0	0	0	0	0
	PBT010	0	0	0	0	0	0	12	5	0	0	0	0	0	0
	PBT	0	0	0	0	0	0	0	13	0	0	0	0	0	0
	PP202	0	0	0	0	0	0	0	0	11	0	0	0	0	0
	PP	0	0	0	0	0	0	0	0	0	16	0	0	0	0
	PS00	0	0	0	0	0	0	0	0	0	0	8	0	0	4
	PS07	0	0	0	0	0	0	0	0	0	0	0	8	0	4
	PS09	0	0	0	0	0	0	0	0	0	0	0	0	16	0
	PS	0	0	0	0	0	0	0	0	0	0	0	0	0	16

very common to find NIR cameras that work between 1000 and 2700 nm, for instance.

Finally, we would like to remark that everyone should look for the hyperspectral application and multivariate/digital image techniques that better suit their purposes. There are many commercial software and libraries that can be used, as well as many types of cameras. Therefore, first, think in the application, aim of the analysis and the scientific problem, and answer yourself these questions:

- *Is hyperspectral imaging really needed?* There are two main domains of hyperspectral applications: the applications in which the structural part of a sample is studied (e.g. distribution of one compound in the surface), and the applications in which the whole object is treated as a homogeneous entity but it is distributed in a surface with different objects (for instance, the case presented in this paper). For the first case, it is obvious that having a distribution of any compound in the surface can only be achieved with imaging techniques. For the second case, the use of imaging techniques really depends on the final purpose pursued and the framework. For instance, in our case the final aim is the implementation of fast NIR imaging methods to classify different plastics moving on a conveyor belt. In principle, a plastic pellet could be considered as a homogeneous surface. This fact is very important in the development of the classification model in such a way that one single NIR spectrum could characterize the whole pellet. Nevertheless, the final application of the classification models will be in a real-time setup where plastics will be passing through a line-by-line NIR imaging

system to check the distribution of different plastics in a portion of the conveyor belt. That is, at the end, one should think that developing a classification or calibration model does not require imaging methods, but the final application (prediction of new samples) does.

- *Which kind of spectral radiation do I need?* This point strongly depends on the final purpose and the chemical complexity of the sample. Thus, it must be studied much before acquiring any camera device. The only sensible advice that can be given on this matter is to deeply study the chemical features of the target pursued. Obviously, the NIR radiation is the workhorse in many applications. Nevertheless, there are many cases in which visible imaging can be more than enough, or cases in which Raman is totally necessary.

Once decided that spectral imaging is the method to be used, there are some other questions that must be solved before acquiring any spectral imaging device. There is a vast amount of devices available in the market and many of them can be adapted to our needs. The selection will strongly depend on the type of the radiation, the spatial and the spectral resolution needed, the size of the objects to be analyzed and the final application of the models developed:

- *Which kind of measurement type do I need?* Traditionally, there are three different types of measurement modalities: point-by-point, line-by-line or imaging-filter based. The point-by-point (whisker broom) is usually very slow and it requires the

movement of the spectrometer in both spatial dimensions. It might be more suitable for studying the microstructure of samples, since the spectral resolution is usually very high and it is used for measuring small areas. The modality that is most commonly adopted is the line-by-line, in which the objects moves along one of the spatial dimensions while the camera obtains one full row of spectra. This modality is fast, allows measuring big surfaces and the spatial and spectral resolutions can be easily tuned. The imaging-filter based modality usually requires that the sample remains still while an image is recorded for every filter. But it can be tuned to work as line-by-line systems.

- Which spatial resolution do I need? It is clear that to characterize the distribution of an active pharmaceutical ingredient in a tablet, a spatial resolution in micrometers is needed. But if the samples are big, spatial resolutions of millimeters might be more than enough.
- Which spectral resolution do I need? Together with the measurement modality, the spectral resolution is a point that strongly depends on the final application. But in this case, it is also a question of how well the chosen radiation discriminates between the elements to quantify or classify. As a matter of fact, Calvini et al. [96] recently published a work in which similar classification performance was obtained using the whole spectrum or several discrete wavelengths. In this case, variable selection methods can be extremely useful to select several discrete wavelengths and implement cameras that, instead of measuring the whole spectrum only measure several discrete wavelengths. The main benefit is that filter-based cameras are usually cheaper and easier to manipulate. The price to pay, though, is that the spectral pre-treatment totally changes in the development of the multivariate models, since now the filters do not give a continuum spectrum.
- Which multivariate models should I use? This point is extremely important since the final result will depend on the type of multivariate model chosen. Several methods have been highlighted in this manuscript regarding exploration (PCA) and resolution (MCR). Regarding quantitation or classification, this manuscript has focused on linear models (PLS-DA). In recent publications a trend of using non-linear models by default (e.g. support vector machines – SVM) can be observed. Nevertheless, as personal opinion, it is preferred to keep the analysis as simpler as possible. If your problem can be solved by linear models, there is no need to go for non-linear modeling. That is, before going to non-linear models, be sure that the correlation between the spectra and the target property do not follow a linear behavior. There are many ways of checking non-linearity in the models, being the non-normal distribution of the residuals and the non-linear relationship in the prediction (predicted vs. theoretical value) the simplest ones to check.
- Which kind of software do I need? As explained before, this strongly depends on our ability to handle big data. If punctual analysis wants to be performed, commercial software can solve the problem. Nevertheless, if the aim is to master in hyperspectral analysis, it can be strongly advised to use software that allows us to program our own routines.

Acknowledgments

This manuscript has been possible thanks to the financial support received from INNOSORT project. INNOSORT is a consortium that brings together technology suppliers, research and knowledge institutions and recipients of waste separation techniques and separated materials. See further information about INNOSORT and partners in <http://innosort.teknologisk.dk/>.

References

- [1] R.A. Schowengerdt, *Remote Sensing*, third ed., Models and Methods for Image Processing, Elsevier, 2006.
- [2] E. Adam, O. Mutanga, D. Rugege, Multispectral and hyperspectral remote sensing for identification and mapping of wetland vegetation: a review, *Wetl. Ecol. Manag.* 18 (2010) 281–296.
- [3] C.A. Lee, S.D. Gasster, A. Plaza, C.I. Chang, B. Huang, Recent developments in high performance computing for remote sensing: a review, *IEEE J. Sel. Top. Appl. Earth Obs. Remote Sens.* 4 (2011) 508–527.
- [4] F.D. van der Meer, H.M.A. van der Werff, F.J.A. van Ruitenbeek, C.A. Hecker, W.H. Bakker, M.F. Noomen, M. van der Meijde, E.J.M. Carranza, J.B. de Smeth, T. Woldai, Multi- and hyperspectral geologic remote sensing: a review, *Int. J. Appl. Earth Obs. Geoinformation* 14 (2012) 112–128.
- [5] J.M. Amigo, J. Cruz, M. Bautista, S. Maspoch, J. Coello, M. Blanco, Study of pharmaceutical samples by NIR chemical-image and multivariate analysis, *TrAC Trends Anal. Chem.* 27 (2008) 696–713.
- [6] C. Gendrin, Y. Roggo, C. Collet, Pharmaceutical applications of vibrational chemical imaging and chemometrics: a review, *J. Pharm. Biomed. Anal.* 48 (2008) 533–553.
- [7] A.A. Gowen, J.M. Amigo, Applications of spectroscopy and chemical imaging in pharmaceuticals, in: J. Popp, V.V. Tuchin, A. Chiou, S.H. Heinemann (Eds.), *Handbook of Biophotonics*, vol. 3, *Photonics in Pharmaceuticals, Bioanalysis and Environmental Research*, Wiley, 2012.
- [8] P.Y. Sacré, C. De Bleye, P.F. Chavez, L. Netchacovitch, P. Hubert, E. Ziemons, Data processing of vibrational chemical imaging for pharmaceutical applications, *J. Pharm. Biomed. Anal.* 101 (2014) 123–140.
- [9] J.M. Amigo, Practical issues of hyperspectral imaging analysis of solid dosage forms, *Anal. Bioanal. Chem.* 398 (2010) 93–109.
- [10] Y. Roggo, A. Edmond, P. Chalus, M. Ulmschneider, Infrared hyperspectral imaging for qualitative analysis of pharmaceutical solid forms, *Anal. Chim. Acta* 535 (2005) 79–87.
- [11] C. Cairós, J.M. Amigo, R. Watt, J. Coello, S. Maspoch, Implementation of enhanced correlation maps in near infrared chemical images: application in pharmaceutical research, *Talanta* 79 (2009) 657–664.
- [12] S. Sasic, D.A. Clark, J.C. Mitchell, M.J. Snowden, Raman line mapping as a fast method for analyzing pharmaceutical bead formulations, *Analyst* 130 (2005) 1530–1536.
- [13] M. Khorasani, J.M. Amigo, J. Sonnergaard, P. Olsen, P. Bertelsen, J. Rantanen, Visualization and prediction of porosity in roller compacted ribbons with near-infrared chemical imaging (NIR-Cl), *J. Pharm. Biomed. Anal.* 109 (2015) 11–17.
- [14] C. Ravn, E. Skibsted, R. Bro, Near-infrared chemical imaging (NIR-Cl) on pharmaceutical solid dosage forms—comparing common calibration approaches, *J. Pharm. Biomed. Anal.* 48 (2008) 554–561.
- [15] J. Cruz, M. Bautista, J.M. Amigo, M. Blanco, Nir-chemical imaging study of acetylsalicylic acid in commercial tablets, *Talanta* 80 (2009) 473–478.
- [16] G.L. Alexandrino, M.R. Khorasani, J.M. Amigo, J. Rantanen, R.J. Poppi, Monitoring of multiple solid-state transformations at tablet surfaces using multi-series near-infrared hyperspectral imaging and multivariate curve resolution, *Eur. J. Pharm. Biopharm.* 93 (2015) 224–230.
- [17] M. Khorasani, J.M. Amigo, C.C. Sun, P. Bertelsen, J. Rantanen, Near-infrared chemical imaging (NIR-Cl) as a process monitoring solution for a production line of roll compaction and tabletting, *Eur. J. Pharm. Biopharm.* 93 (2015) 293–302.
- [18] J.M. Amigo, I. Martí, A. Gowen, Hyperspectral imaging and chemometrics. a perfect combination for the analysis of food structure, composition and quality, *Data Handl. Sci. Technol.* (2013) 343–370.
- [19] G. ElMasry, M. Kamruzzaman, D.W. Sun, P. Allen, Principles and applications of hyperspectral imaging in quality evaluation of agro-food products: a review, *Crit. Rev. Food Sci. Nutr.* 52 (2012) 999–1023.
- [20] G. Elmasry, N. Wang, A. ElSayed, M. Ngadi, Hyperspectral imaging for nondestructive determination of some quality attributes for strawberry, *J. Food Eng.* 81 (2007) 98–107.
- [21] P.M. Mehl, Y.-R. Chen, M.S. Kim, D.E. Chan, Development of hyperspectral imaging technique for the detection of apple surface defects and contaminations, *J. Food Eng.* 61 (2004) 67–81.
- [22] G. Fox, M. Manley, Applications of single kernel conventional and hyperspectral imaging near infrared spectroscopy in cereals, *J. Sci. Food Agric.* 94 (2014) 174–179.
- [23] D. Lorente, N. Aleixos, J. Gomez-Sanchis, S. Cubero, O.L. Garcia-Navarrete, J. Blasco, Recent advances and applications of hyperspectral imaging for fruit and vegetable quality assessment, *Food Bioprocess Technol.* 5 (2012) 1121–1142.
- [24] D. Sun, *Hyperspectral Imaging for Food Quality Analysis and Control*, Elsevier Inc, 2010.
- [25] A.A. Gowen, C.P. O'Donnell, P.J. Cullen, G. Downey, J.M. Frias, Hyperspectral imaging – an emerging process analytical tool for food quality and safety control, *Trends Food Sci. Technol.* 18 (2007) 590–598.
- [26] J.H. Cheng, D.W. Sun, Hyperspectral imaging as an effective tool for quality analysis and control of fish and other seafoods: current research and potential applications, *Trends Food Sci. Technol.* 37 (2014) 78–91.
- [27] S. Cubero, N. Aleixos, E. Molto, J. Gómez-Sanchis, J. Blasco, Advances in machine vision applications for automatic inspection and quality evaluation of

- fruits and vegetables, *Food Bioprocess Technol.* 4 (2011) 487–504.
- [28] I. Kim, M.S. Kim, Y.R. Chen, S.G. Kong, Detection of skin tumors on chicken carcasses using hyperspectral fluorescence imaging, *Trans. ASAE* 47 (2004) 1785–1792.
- [29] Y.Z. Feng, D.W. Sun, Application of hyperspectral imaging in food safety inspection and control: a review, *Crit. Rev. Food Sci. Nutr.* 52 (2012) 1039–1058.
- [30] S. Mahesh, D.S. Jayas, J. Paliwal, N.D.G. White, Hyperspectral imaging to classify and monitor quality of agricultural materials, *J. Stored Prod. Res.* 61 (2015) 17–26.
- [31] Z. Xiong, D.W. Sun, X.A. Zeng, A. Xie, Recent developments of hyperspectral imaging systems and their applications in detecting quality attributes of red meats: a review, *J. Food Eng.* 132 (2014) 1–13.
- [32] K. Flynn, R. O'Leary, C. Roux, B.J. Reedy, Forensic analysis of bicomponent fibers using infrared chemical imaging, *J. Forensic Sci.* 51 (2006) 586–596.
- [33] G.J. Edelman, E. Gaston, T.G. van Leeuwen, P.J. Cullen, M.C.G. Alders, Hyperspectral imaging for non-contact analysis of forensic traces, *Forensic Sci. Int.* 223 (2012) 28–39.
- [34] M.A.F. De La Ossa, C. García-Ruiz, J.M. Amigo, Near infrared spectral imaging for the analysis of dynamite residues on human handprints, *Talanta* 130 (2014) 315–321.
- [35] M.T. Fernández de la Ossa, J.M. Amigo, C. García-Ruiz, Detection of residues from explosive manipulation by near infrared hyperspectral imaging: a promising forensic tool, *Forensic Sci. Int.* 242 (2014) 228–235.
- [36] C.S. Silva, M.F. Pimentel, R.S. Honorato, C. Pasquini, J.M. Prats-Montalbán, A. Ferrer, Near infrared hyperspectral imaging for forensic analysis of document forgery, *Analyst* 139 (2014) 5176–5184.
- [37] K. Flynn, R. O'Leary, C. Lennard, C. Roux, B.J. Reedy, Forensic applications of infrared chemical imaging: multi-layered paint chips, *J. Forensic Sci.* 50 (2005) 832–841.
- [38] G.L. Lu, B.W. Fei, Medical hyperspectral imaging: a review, *J. Biomed. Opt.* 19 (2014).
- [39] R.F. Kokaly, G.P. Asner, S.V. Ollinger, M.E. Martin, C.A. Wessman, Characterizing canopy biochemistry from imaging spectroscopy and its application to ecosystem studies, *Remote Sens. Environ.* 113 (2009) S78–S91.
- [40] C.G. Zhang, H. Wang, J.F. Huang, Q. Gao, The visible to the near infrared narrow band acousto-optic tunable filter and the hyperspectral microscopic imaging on biomedicine study, *J. Opt. UK* 16 (2014).
- [41] M.E. Klein, B.J. Aalderink, R. Padoan, G. de Bruin, T.A.G. Steemers, Quantitative hyperspectral reflectance imaging, *Sensors* 8 (2008) 5576–5618.
- [42] F. Rosi, C. Miliani, R. Braun, R. Harig, D. Sali, B.G. Brunetti, A. Sgamellotti, Noninvasive analysis of paintings by mid-infrared hyperspectral imaging, *Angew. Chem. Int. Ed.* 52 (2013) 5258–5261.
- [43] Z.M. Xu, E.Y. Lam, Image reconstruction using spectroscopic and hyperspectral information for compressive terahertz imaging, *J. Opt. Soc. Am. A* 27 (2010) 1638–1646.
- [44] C.M. Wang, S.C. Yang, P.C. Chung, C.I. Chang, C.S. Lo, C.C. Chen, C.W. Yang, C.H. Wen, Orthogonal subspace projection-based approaches to classification of MR image sequences, *Comput. Med. Imag. Graph.* 25 (2001) 465–476.
- [45] S. Sasic, Y. Ozaki, Raman, Infrared, and Near-infrared Chemical Imaging, Wiley, 2010.
- [46] J.A.F. Pierna, P. Vermeulen, O. Amand, A. Tossens, P. Dardenne, V. Baeten, NIR hyperspectral imaging spectroscopy and chemometrics for the detection of undesirable substances in food and feed, *Chemom. Intell. Lab.* 117 (2012) 233–239.
- [47] P. Geladi, H. Grahn, M. Manley, Data analysis and chemometrics for hyperspectral imaging, in: S. Sasic, Y. Ozaki (Eds.), Raman, Infrared, and Near-infrared Chemical Imaging, Wiley, 2010.
- [48] C.I. Chang, X. Jiao, C.C. Wu, Y. Du, M.L. Chang, A review of unsupervised spectral target analysis for hyperspectral imagery, *Eurasip J. Adv. Signal Process.* 2010 (2010).
- [49] D.M. Haaland, H.D.T. Jones, M.H. Van Benthem, M.B. Sinclair, D.K. Melgaard, C.L. Stork, M.C. Pedroso, P. Liu, A.R. Brasier, N.L. Andrews, D.S. Lidke, Hyperspectral confocal fluorescence imaging: exploring alternative multivariate curve resolution approaches, *Appl. Spectrosc.* 63 (2009) 271–279.
- [50] J.M. Prats-Montalbán, A. de Juan, A. Ferrer, Multivariate image analysis: a review with applications, *Chemom. Intell. Lab.* 107 (2011) 1–23.
- [51] B. Boldrin, W. Kessler, K. Rebnera, R.W. Kessler, Hyperspectral imaging: a review of best practice, performance and pitfalls for in-line and on-line applications, *J. Near Infrared Spectrosc.* 20 (2012) 483–508.
- [52] M. Vidal, J.M. Amigo, Pre-processing of hyperspectral images. Essential steps before image analysis, *Chemom. Intell. Lab.* 117 (2012) 138–148.
- [53] G. Bonifazi, L. Damiani, S. Serranti, E.J. Bakker, P.C. Rem, Innovative sensing technologies applied to post-consumer polyolefins recovery, *Metal. Int.* 14 (2009) 5–10.
- [54] S. Serranti, A. Gargiulo, G. Bonifazi, Characterization of post-consumer polyolefin wastes by hyperspectral imaging for quality control in recycling processes, *Waste Manag.* 31 (2011) 2217–2227.
- [55] S. Serranti, A. Gargiulo, G. Bonifazi, Classification of polyolefins from building and construction waste using NIR hyperspectral imaging system, *Resour. Conserv. Recycl.* 61 (2012) 52–58.
- [56] A. Ulrici, S. Serranti, C. Ferrari, D. Cesare, G. Foca, G. Bonifazi, Efficient chemometric strategies for PET-PLA discrimination in recycling plants using hyperspectral imaging, *Chemom. Intell. Lab.* 122 (2013) 31–39.
- [57] C.A. de Wit, An overview of brominated flame retardants in the environment, *Chemosphere* 46 (2002) 583–624.
- [58] Shimadzu, Identification of Brominated Flame Retardants in Polymers, Shimadzu News, Shimadzu, 2005, pp. 10–11.
- [59] S. Kikuchi, K. Kawauchi, S. Ooki, M. Kurosawa, H. Honjoh, T. Yagishita, Non-destructive rapid analysis of brominated flame retardants in electrical and electronic equipment using Raman spectroscopy, *Anal. Sci.* 20 (2004) 1111–1112.
- [60] M. Stepputat, R. Noll, On-line detection of heavy metals and brominated flame retardants in technical polymers with laser-induced breakdown spectrometry, *Appl. Opt.* 42 (2003) 6210–6220.
- [61] A. Golloch, D. Siegmund, Sliding spark spectroscopy – rapid survey analysis of flame retardants and other additives in polymers, *Fresen. J. Anal. Chem.* 358 (1997) 804–811.
- [62] C. Gallen, A. Banks, S. Brandsma, C. Baduel, P. Thai, G. Eaglesham, A. Heffernan, P. Leonards, P. Bainton, J.F. Mueller, Towards development of a rapid and effective non-destructive testing strategy to identify brominated flame retardants in the plastics of consumer products, *Sci. Total Environ.* 491 (2014) 255–265.
- [63] M. Schlummer, F. Brandl, A. Maurer, R. van Eldik, Analysis of flame retardant additives in polymer fractions of waste of electric and electronic equipment (WEEE) by means of HPLC-UV/MS and GPC-HPLC-UV, *J. Chromatogr. A* 1064 (2005) 39–51.
- [64] J. Burger, P. Geladi, Hyperspectral NIR image regression part II: dataset pre-processing diagnostics, *J. Chemom.* 20 (2006) 106–119.
- [65] J. Burger, P. Geladi, Hyperspectral NIR image regression part I: calibration and correction, *J. Chemom.* 19 (2005) 355–363.
- [66] P. Geladi, J. Burger, T. Lestander, Hyperspectral imaging: calibration problems and solutions, *Chemom. Intell. Lab.* 72 (2004) 209–217.
- [67] Phyton, <https://www.python.org/>.
- [68] RStudio, <http://www.rstudio.com/>.
- [69] I. The MathWorks, <http://se.mathworks.com/>.
- [70] M.T.b.E.R. Inc., http://www.eigenvector.com/software/mia_toolbox.htm.
- [71] ENVI, <http://www.exelisvis.com/ProductsServices/ENVIProducts/ENVI.aspx>.
- [72] J.M. Amigo, C. Ravn, N.B. Gallagher, R. Bro, A comparison of a common approach to partial least squares-discriminant analysis and classical least squares in hyperspectral imaging, *Int. J. Pharm.* 373 (2009) 179–182.
- [73] E.R. Inc., <http://eigenvector.com/>.
- [74] I. The MathWorks, Image Processing Toolbox™, 2015.
- [75] F.M. Mirabella, Internal-reflection spectroscopy, *Appl. Spectrosc. Rev.* 21 (1985), 45–178.
- [76] A. Rinnan, F. van den Berg, S.B. Engelsen, Review of the most common pre-processing techniques for near-infrared spectra, *TrAC Trend Anal. Chem.* 28 (2009) 1201–1222.
- [77] B.D. Prakash, Y.C. Wei, A fully automated iterative moving averaging (AIMA) technique for baseline correction, *Analyst* 136 (2011) 3130–3135.
- [78] S.X. He, W. Zhang, L.J. Liu, Y. Huang, J.M. He, W.Y. Xie, P. Wu, C.L. Du, Baseline correction for Raman spectra using an improved asymmetric least squares method, *Anal. Methods UK* 6 (2014) 4402–4407.
- [79] A. de Juan, R. Tauler, Chemometrics applied to unravel multicomponent processes and mixtures, *Anal. Chim. Acta* 500 (2003) 195–210.
- [80] A. de Juan, R. Tauler, Multivariate curve resolution (MCR) from 2000: progress in concepts and applications, *Crit. Rev. Anal. Chem.* 36 (2006) 163–176.
- [81] J.M. Amigo, C. Ravn, Direct quantification and distribution assessment of major and minor components in pharmaceutical tablets by NIR-chemical imaging, *Eur. J. Pharm. Sci.* 37 (2009) 76–82.
- [82] J. Felten, H. Hall, J. Jaumot, R. Tauler, A. de Juan, A. Gorzsas, Vibrational spectroscopic image analysis of biological material using multivariate curve resolution-alternating least squares (MCR-ALS), *Nat. Protoc.* 10 (2015) 217–240.
- [83] M. Boiret, A. de Juan, N. Gorretta, Y.M. Ginot, J.M. Roger, Distribution of a low dose compound within pharmaceutical tablet by using multivariate curve resolution on Raman hyperspectral images, *J. Pharm. Biomed. Anal.* 103 (2015) 35–43.
- [84] S. Piqueras, L. Duponchel, M. Offroy, F. Jamme, R. Tauler, A. de Juan, Chemometric strategies to unmix information and increase the spatial description of hyperspectral images: a single-cell case study, *Anal. Chem.* 85 (2013) 6303–6311.
- [85] S. Piqueras, J. Burger, R. Tauler, A. de Juan, Relevant aspects of quantification and sample heterogeneity in hyperspectral image resolution, *Chemom. Intell. Lab.* 117 (2012) 169–182.
- [86] S. Piqueras, L. Duponchel, R. Tauler, A. de Juan, Resolution and segmentation of hyperspectral biomedical images by multivariate curve resolution-alternating least squares, *Anal. Chim. Acta* 705 (2011) 182–192.
- [87] A. de Juan, J. Jaumot, R.A. Tauler, Multivariate Curve Resolution (MCR). Solving the mixture analysis problem, *Anal. Methods UK* 6 (2014) 4964–4976.
- [88] A. de Juan, M. Maeder, T. Hancewicz, R. Tauler, Use of local rank-based spatial information for resolution of spectroscopic images, *J. Chemom.* 22 (2008) 291–298.
- [89] M. Barker, W. Rayens, Partial least squares for discrimination, *J. Chemom.* 17 (2003) 166–173.
- [90] I.G. Chong, C.H. Jun, Performance of some variable selection methods when multicollinearity is present, *Chemom. Intell. Lab.* 78 (2005) 103–112.
- [91] D. Lorente, J. Blasco, A.J. Serrano, E. Soria-Olivas, N. Aleixos, J. Gomez-Sanchis, Comparison of ROC feature selection method for the detection of decay in citrus fruit using hyperspectral images, *Food Bioprocess Technol.* 6 (2013) 3613–3619.

- [92] J. Demsar, Statistical comparisons of classifiers over multiple data sets, *J. Mach. Learn. Res.* 7 (2006) 1–30.
- [93] D.J. Hand, Assessing the performance of classification methods, *Int. Stat. Rev.* 80 (2012) 400–414.
- [94] R.C. Gonzalez, R.E. Woods, E.L. Eddins, *Digital Image Processing Using MATLAB*, Gatesmark Publishing, 2009.
- [95] J. Canny, A computational approach to edge-detection, *IEEE Trans. Pattern Anal.* 8 (1986) 679–698.
- [96] R. Calvini, A. Ulrici, J.M. amigo, Practical comparison of sparse methods for classification of Arabica and Robusta coffee species using near infrared hyperspectral imaging, *Chemom. Intell. Lab.* 146 (2015) 503–511.



Dr. José Manuel Amigo Born in 1978. He obtained his PhD (Cum Laude) in Chemistry from the Autonomous University of Barcelona, Spain. Since 2007 he has been employed at the Department of Food Science, Spectroscopy and Chemometrics group of the University of Copenhagen, Denmark, as associate professor. Current research interests include hyperspectral and digital image analysis, chromatographic data analysis, Food Sciences, environmental modeling, curve resolution and teaching chemometrics. He has authored more than 95 publications (70+ peer-reviewed papers, books, book chapters, proceedings, etc.) and given more than 40 conferences at international meetings. Jose has supervised or is currently supervising several Masters, Post Docs and PhD students and he is an editorial board member of four scientific journals within chemometrics, pharmaceutical sciences and analytical chemistry. Moreover, he has recently received the “2014 Chemometrics and Intelligent Laboratory Systems Award”.



Dr. Hamid Babamoradi Born in 1982, he obtained his PhD in Chemometrics and Statistical Process Control from University of Copenhagen, Denmark. Since end of 2012, he has been employed as postdoctoral scholar at Spectroscopy and Chemometrics section, Department of Food Science, University of Copenhagen, Denmark. Current research interests include hyperspectral and digital image analysis, multivariate statistical process control (MSPC), dairy process control. He has authored multiple peer-reviewed papers and been working on multiple industrial projects (such as automation of waste sorting and dairy process control). He has also been involved in teaching MSPC, PAT, and Chemometric courses.



Dr. Saioa Elcoroaristizabal Born in 1983, she obtained her International Ph.D. in Environmental Engineering from the University of the Basque Country, Spain, in 2015. She obtained her Chemical Engineering degree in 2007 and developed her research skills through different projects related to environmental engineering carried out for private and public entities. In 2010, she obtained her Ms.C in Environmental Engineering, acquiring additional theoretical and practical background on chemometrics during several research stays. Since then, she has authored and co-authored several peer-review papers and presented her research findings in several national and international conferences. She has also been involved in teaching in the degree of Environmental Engineering at the University of the Basque Country, Spain.